Exploring Molecular Traffic Jams: Single-Molecule Imaging of Replication-Transcription Conflicts in *E. coli*

Rachel Hope

MSc by Research

University of York

Biology

October 2024

Abstract

The frequency of replication-transcription conflicts offers an interesting direction of study, with cells able to overcome these occurrences and maintain cell viability despite the ubiquitous nature of replication fork stalling. However, the mechanism of the replisome as it encounters these blocks is not fully understood, particularly when multiple replisomes converge conflict sites. This project aimed to uncover novel insights into the dynamics of the replisome as it encounters an array of lac repressor-operator complexes, mimicking the collisions between replication and transcription machinery and set a baseline for future study of replication conflicts under genetic perturbation. Single-molecule, dual-colour Slimfield imaging was used to quantify the stoichiometry and localisation of core replisome components and the Lac repressor. This included the replisome proteins DnaE and DnaQ, responsible for polymerase and exonuclease activity of the replisome respectively.

The percentage of cells with DnaE foci was reduced from approximately 74±0.01% to 60±0.01% upon expression of the Lac repressor, with 21% of cells forming repressor-operator complexes. However, only 3% of cells demonstrated colocalisation between the replisome component and the array. Within this population, there was a significant increase in DnaE and DnaQ stoichiometry over time, peaking at averages of 12.7±1.84 and 10.2±1.2 respectively. Following induction of LacI-mCherry, there was an increase in cells with DnaT foci from approximately 28±0.01% to 39±0.07% These results highlight the efficiency of the replication and repair mechanisms developed by *E. coli*. Furthermore, they point to a novel model of replication block in which consecutive replisomes stall and stack up at the site of more persistent conflicts, leading to dissociation of the complex and restart mediated by the replication restart proteins. Increasing the understanding of fundamental bacterial cell biology processes, including the mechanism of DNA replication, has the potential to aid in the identification of targets for the development of new antibiotics.

Declaration

I declare that this thesis is a presentation of original work, and I am the sole author. I acknowledge the contribution of Aisha Syeda (Biology, University of York) in running the analysis scripts to determine copy numbers. This work has not previously been presented for a degree or other qualification at this University or elsewhere. All sources are acknowledged as references.

Table of Contents

Acknowledgements

I would like to thank my supervisors, Mark Leake and Aisha Syeda for their guidance and advice throughout the MSc by Research. This project would not have been possible without their combined expertise in bacterial replication and microscopy. In particular, I would like to thank Aisha for the excellent lab-based training I received throughout this year. I am also grateful to Aisha for carrying out the copy number quantification of LacI-mCherry from my imaging datasets. I would also like to thank the flow cytometry team at the technology facility who enabled me to carry out important experiments for this project without having previous experience in the methods. In addition, the feedback of Michelle Hawkins was crucial to the development of this project as my TAP member. Lastly, the encouragement and support to the Physics of Life group was vital to the completion of the research project.

List of Tables and Figures

List of Tables

List of Figures

22. *Cell area in pixels of AS1000 (DnaE-mYPet, LacI-mCherry).*
23. *Cell area in pixels of AS996 (DnaQ-mYPet, LacI-mCherry).*
24. *DnaT total stoichiometry RH23 (*mGFP-dnaT*, lacI-mCherry).*
25. *DnaT total stoichiometry RH25 (*mGFP-dnaT*, empty vector).*
26. *OD600 over the course of 19 hours (plotted in minutes) for all strains used in the study.*
27. *Flow cytometry plots for AS985 - empty vector control and RH28 - repressor strain.*
28. *Dynamics of the replisome as it reaches the block.*

Introduction

DNA replication is an essential process in living organisms. However, this process often comes into conflict with other biological mechanisms such as transcription. In bacteria, if conflicts cannot be resolved, the failure to replicate the DNA reduces the chance of the survival of the cell. As a result, bacteria have a range of mechanisms to overcome or reduce the likelihood of conflicts. This project explores the dynamics of the replication machinery as it encounters obstacles to progression.

Background

The accurate duplication of the chromosome is essential for preserving genome stability and preventing the accumulation of undesirable mutations, with the mechanisms of DNA replication highly conserved throughout evolution (O'Donnell, Langston and Stillman, 2013). Multiple proteins coordinate the three stages of bacterial DNA replication to ensure the process's precise and timely initiation, elongation and eventual termination, with two sister replisomes carrying out bidirectional replication starting from a single origin on the chromosome (figure 1) (Prescott and Kuempel, 1972). In contrast with eukaryotic replication, bacteria may initiate multiple rounds of replication before undergoing cell division (Krystian Łazowski, Woodgate and Fijalkowska, 2024). This enables complete copies of the genome to be inherited by daughter cells despite the rate of cell division being faster than the time required for duplication of the chromosome (Berger and Rein, 2023).

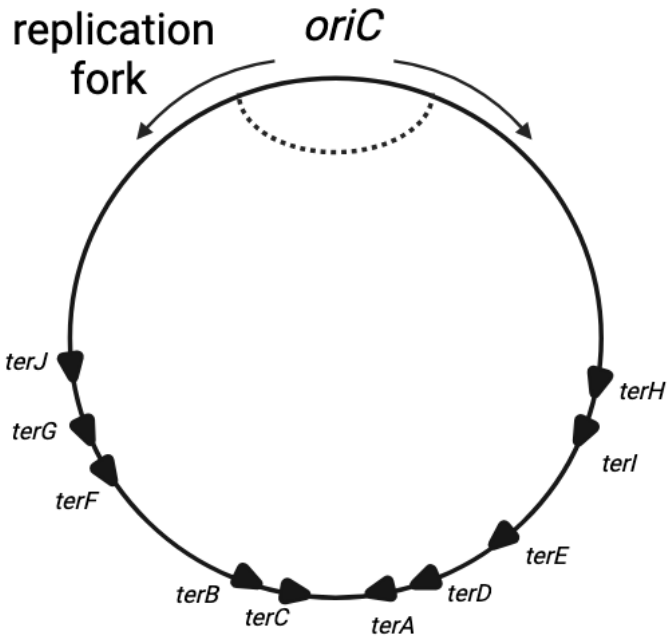

Figure 1. E. coli replication: E. coli replicates the genome bidirectionally starting from the origin (oriC) and ending at a loosely defined terminus region spanning several ter sites. Adapted from (Beattie and Reyes-Lamothe, 2015).

DNA replication is characterised by the synthesis of new strands in the 5' to 3' direction. The antiparallel orientation of the two strands necessitates differing duplication mechanisms, with the leading strand being synthesised continuously and the lagging strand synthesised discontinuously via the formation of Okazaki fragments. However, this traditional model of DNA replication as a semi-discontinuous process has been challenged by *in vivo* studies demonstrating discontinuous leading strand replication even in the absence of DNA damaging agents. Furthermore, proteins involved in replication restart are essential in bacterial genomes, indicating a frequent need for the rescue of stalled or dissociated replisomes (Mangiameli et al., 2017), with the *E. coli* replication fork stalling and replication restart occurring at least once per cell cycle (Cox et al., 2000).

Numerous studies (Brüning and Marians, 2021; Goehring et al., 2023; Mangiameli et al., 2017) have outlined the various obstacles the replisome faces as it translocates across the chromosome, the most frequent of which are nucleoprotein complexes bound by DNA. Therefore, the pervasive nature of replication conflicts during the bacterial cell cycle may

explain the lack of continuity observed in the DNA duplication of living cells. However, our understanding of the dynamics of replisomes as they encounter such blocks, particularly in the context of multiple initiation events, is limited. *E. coli, which has a single, circular chromosome, is a key model organism for understanding the mechanisms by which the accurate duplication of DNA can be maintained despite the high potential for conflicts. Strains in this project are derivatives of the strain MG1655 which has a genome of approximately 4.6 Mb (Blattner, 1997).*

Importance

Antimicrobial resistance (AMR) is a growing threat to global public health, with the rise of multidrug-resistant (MDR) pathogens making the treatment of infections increasingly challenging. Both RNA transcription and DNA replication are key processes targeted by existing antibiotics. DNA replication is inhibited indirectly by targeting enzymes such as DNA gyrases, which are involved in managing the supercoiling of DNA during replication. However, as Santos and Lamers (2020) outlined, no antibiotics currently target the replisome. Despite this, the replisome has emerged as a potential target for antibiotic development in recent decades (Robinson et al., 2012), with replicative proteins found to be highly conserved across bacterial species. A particularly promising target is the replicative polymerase DnaE. DnaE demonstrates strong potential for drug development in part due to the structural differences between prokaryotic and eukaryotic DNA polymerases (McHenry, 2011), making it possible to inhibit bacterial replication without damaging human cells. By advancing research into the fundamentals of the structure and function of the replisome, there is potential to aid in the development of novel antibiotics that directly target bacterial DNA replication.

The replisome

Replisomes are multi-protein molecular machines (figure 2) driving DNA replication with exceptional speed and accuracy. The replisome separates the DNA double helix to facilitate the synthesis of complementary copies of each strand. This mechanism creates junctions known as replication forks. Replisome components are capable of engaging and disengaging from the DNA, whilst maintaining their association to the replication fork. In *E. coli*, two sister replisomes assemble at the origin of replication (oriC) following replication initiation and proceed to replicate the chromosome bidirectionally. Once the entire genome has been

duplicated, the replisomes converge and terminate upon reaching the specific Tus sites at the terminus (figure 1). Strand separation at the origin is carried out by the initiator protein DnaA, allowing assembly of the replisome proteins and helicase DnaB (Margulies and Kaguni, 1996). During this process, DnaC binds to DnaB and facilitates its loading onto the DNA duplex. DnaB can then unwind the DNA duplex through ATP hydrolysis. This allows access to single-stranded DNA (ssDNA) for the DNA polymerase III holoenzyme (Pol III HE) for the synthesis of nascent DNA (Beattie and Reyes-Lamothe, 2015). Pol III HE consists of three subassemblies: The core polymerase complex, the β2 sliding clamp and the clamp loader complex (O'Donnell, 2006). The core complex is encoded by the *dnaE* (α-subunit)*, dnaQ* (ε-subunit) and *holE* (θ-subunit) genes. The active site of the polymerase is located in the α-subunit, exonuclease proofreading in the 3'-5' direction is carried out by the ε-subunit (Ozawa et al., 2013) and although the role of the θ-subunit has not been well established, it is thought to aid in stabilising the proofreading unit (Taft-Benz and Schaaper, 2004). Another essential protein involved in DNA replication is the ssDNA-binding protein (SSB). SSB coats ssDNA in order to prevent pairing between bases of the same strand and the resulting formations, such as DNA hairpins (Grieb et al., 2017), as well as to protect the ssDNA from nucleolytic attack (Marceau, 2012). SSB also plays a vital role during replication in organising the interactions between proteins and DNA within the replisome (Antony and Lohman, 2019). Of the core complex, this thesis focuses on the α (polymerase) and ε (exonuclease) subunits encoded by *dnaE* and *dnaQ*, respectively.

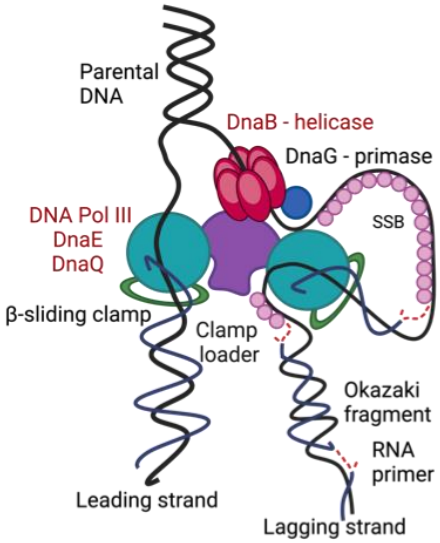

Figure 2. The structure of the replisome. Two DNA Polymerase complexes carry out replication of the leading strand and the lagging strand. Proteins of interest for this project are shown in red. DnaE and DnaQ are core replisome components, encoding the polymerase. DnaB acts as a helicase and anchors the replisome to the chromosome. Adapted from (Langston, Indiani and O'Donnell, 2009).

Previous single-molecule studies have aimed to explore the architecture of the replisome *in vivo* in order to build on *in vitro* studies that may not show a clear picture of the structure and mechanism of the replisome in living cells, such as the presence of additional replisome components copies at replication forks. Reyes-Lamothe et al. (2010) used slimfield microscopy to determine that a single replication fork has three copies of both the ε and α subunits of the replisome. This corresponds to trimeric structures and was also found to be the case for the τ subunit (the clamp loader). By contrast, the δ subunit, which is another essential component of the clamp loader, was present as a monomer, and the helicase DnaB exhibited a stoichiometry of six, consistent with the expected structure as a hexamer. The consistency of single-molecule observations with the replisome structure determined by *in vitro* studies highlights the efficacy of single-molecule slimfield imaging. Furthermore, the findings of this study concerning the presence of three rather than the expected two molecules of the replicative polymerase in active replisomes demonstrate the importance of non-invasive *in vivo* approaches for determining the assembly of molecular machines in living cells.

Replication-transcription conflicts

Replication can be disrupted by DNA-binding proteins present on the chromosome. Notably, transcription complexes pose a particular problem to replisome progression (Guy et al., 2009). Both transcription and replication are highly processive and adhere to 5’ to 3’ polarity when moving along the DNA, with the RNAP complex acting to carry out transcription, requiring access to the same DNA template necessary for genome duplication (Hamperl and Cimprich, 2016; Merrikh et al., 2012).The simultaneous activity of replication and transcription, combined with the faster translocation rate along the chromosome of the replisome (the replisome is greater than 10-fold faster than RNAP (Wolak et al., 2020)) results in a lack of spatial or temporal separation between the two processes. This gives rise to inevitable collisions between the two complexes. The presence of stalled RNAPs at regulatory sequences or sites of DNA damage amplifies this problem. In particular, the backward translocation of stalled RNAPs unable to restart transcription presents a barrier to both replisomes and transcription complexes (Trautinger et al., 2005). As a result, arrays of immobile RNAPs may form on the chromosome.

The severity of collisions between the transcription and replication machinery and the resulting effect on the stability of the genome is dependent on both the orientation in which the complexes meet and the type of transcriptional block. Collisions can be head-on or co-directional (figure 3), with head-on collisions being the more significant cause of alterations to the genome (Mirkin and Mirkin, 2005; Sankar et al., 2016; Srivatsan et al., 2010). Head-on collisions may lead to the inactivation of helicases as they unwind parental DNA strands or the accumulation of positive DNA supercoils as the replisome converges with RNAP, resulting in the inhibition of both mechanisms. Conversely, collisions in the co-directional orientation can lead to the displacement of RNAP and the consequent continuation of the replisome along the DNA. However, these collisions also have the potential to impact genome stability, particularly in cases of more persistent transcriptional blocks (Hamperl and Cimprich, 2016).

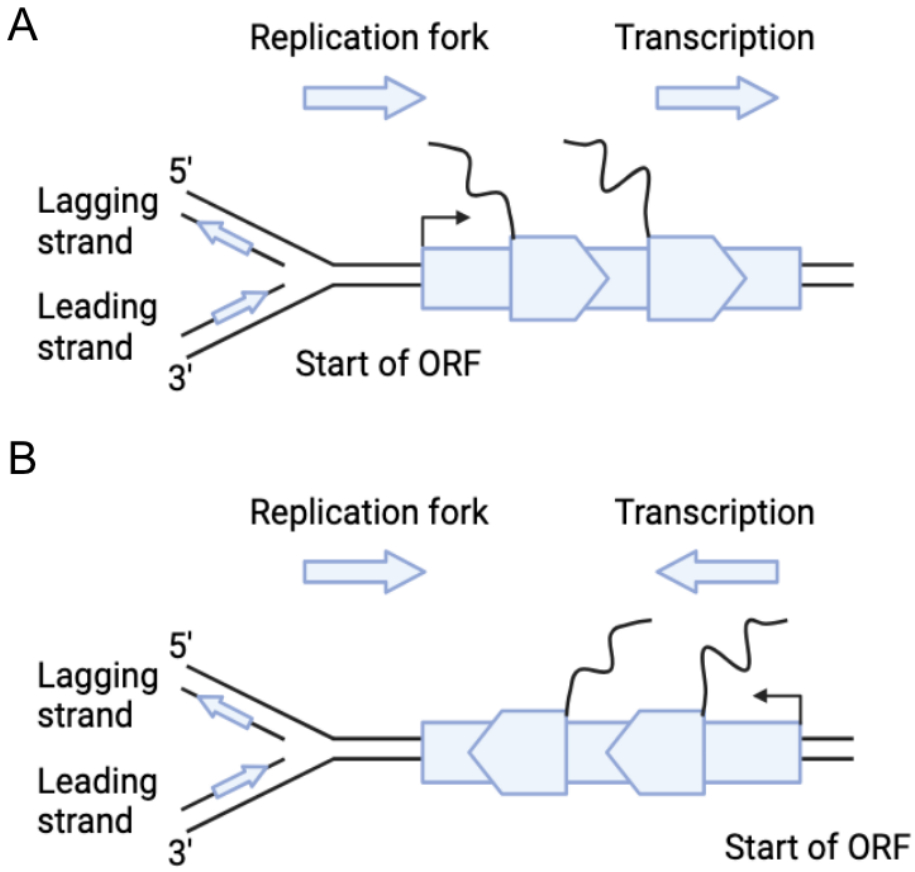

Figure 3. Illustration of conflicts due to transcriptional orientation with respect to the replisome. A. Co-directional conflicts: The replication fork travels in the same direction as RNAP carrying out transcription. B. Head-on conflicts: The replication fork travels in the opposite direction to transcription. Adapted from (Lin and Pasero, 2017).

Although some existing studies looking at replication-transcription conflicts *in vitro* suggested co-directional collisions between these machineries are not harmful to replisome progression (Pomerantz and O'Donnell, 2008), current literature demonstrates that stalling events at co-directionally oriented genes increase when genes involved in conflict resolution are not functional (Merrikh et al., 2015). As a result of the 10-fold difference in translocation rates between DNA Polymerase and RNA Polymerase, codirectional collisions are inevitable in E. coli (Wolak et al., 2020). According to Dutta et al. (2011), codirectional collisions between the replisome and backtracked transcription elongation complexes frequently lead to double-strand breaks (DSB). Furthermore, Nudler (2012) presented a model based on intro observations in which the displacement of RNAP resulting from a co-directional collision promotes the "jumping" of DNAP III (DNA Polymerase III) to the 3' end of the nascent transcript, which acts as a primer. The 'jump'

leads to a single stranded break which under normal conditions may be repaired before the next round of replication. However, in the presence of high rates of backtracking, the DNA repair mechanism is not robust enough to repair the break, resulting in the subsequent round of replication creating a DSB.

This indicates that the replisome may be inefficient in displacing RNAPs without the activity of additional factors. However, it has also been proposed that co-directional collisions may be resolved by the replisome itself, with the mRNA transcript acting as a primer (Pomerantz and O'Donnell, 2008). Brüning and Marians (2021) suggest that mRNA takeover is predominantly used to resolve the presence of single RNAPs, with more complex transcriptional blocks requiring the synthesis of new primers downstream of the complex. Even so, they presented the displacement of RNAP as a necessity for bypassing single and complex RNAP blocks, with the replisome 'skipping' over the obstacle.

Therefore, given the inevitability of these conflicts resulting from the shared DNA template, *E. coli* has developed several mechanisms to reduce the frequency of replication-transcription conflicts. One example is that of genome organisation. Almost all bacteria show a co-directional orientation between replication and the highly transcribed rRNA genes. Similarly, although approximately only 55% of *E. coli* genes exhibit a co-directional orientation (Blattner, 1997), this figure increases to around 70% for essential genes (Eduardo and Danchin, 2003) and 100% for the rRNA operons (Guy and Roten, 2004). The inversion of rRNA genes leads to the disruption of replication forks (Srivatsan et al., 2010), indicating a reduction in fitness as the driver of the orientation bias. *E. coli* is also able to minimise conflicts through RNAP modulators. RNAP modulators act to remove or destabilise transcription barriers. This includes transcription factors such as DskA and GreA/B, which have been shown to play a role in removing replication barriers. *In vitro* studies on linear phage DNA demonstrate that DksA is involved in preventing transcription elongation complex stalling (Perederina et al., 2004). In addition, there is evidence of the importance of DksA in *in vivo* replication-transcription conflicts (Tehranchi et al., 2010).

A third key mechanism in the reduction of collisions is the removal of roadblocks by accessory helicases. *E. coli* has been shown to maintain cell viability through the cooperative action of

the accessory replicative helicases DinG, Rep and UvrD (Boubakri et al., 2010). *In vivo* evidence points to a role for UvrD and Rep in removing DNA-bound proteins, with increased sensitivity of double mutants to the presence of lac repressor-operator complexes (Guy et al., 2009). *In vitro* studies indicate that the removal of RecA filaments from DNA generated during the RecFOR pathway is mediated by UvrD (Lestini and Michel, 2008), suggesting it may also play an important role in the restart of stalled replication forks *in vivo*. It has therefore been established that the accessory helicases are likely to be involved both in the removal of RNAP and the restart of stalled forks.

Replication fork stalling and restart

Despite mechanisms to mitigate collisions between the transcription and replication machinery, conflicts still occur. Following a collision with RNAPs, the replisome may stall at the site of the conflict, with numerous studies identifying transcription as a significant source of replisome stalling in bacteria ((Dutta et al., 2011; Mangiameli et al., 2017; Merrikh et al., 2011). Even in wild-type *E. coli*, replication forks have been found to stall at least once per cell cycle, with earlier estimates of the frequency of replication restart events from once per cell cycle to once in seven generations (Cox et al., 2000). However, more recent studies indicate replication restart following conflicts between the replisome and other cellular machinery occur multiple times per cell cycle (Mangiameli et al., 2017), with estimates of complete dissociation of the replisome from the DNA template as frequent as five times over the course of a single round of replication.

In the case that the replisome remains stalled following a collision, it may disassemble from the DNA template. This is evident from the presence of primosome proteins at sites of conflict (Merrikh et al., 2011). The *E. coli* primosome consists of a complex of seven proteins involved in the priming of DNA for replication through the generation of RNA primers of single-stranded DNA. This includes the DnaG primase, DnaB helicase and DnaC helicase. However, the primosome also plays a crucial role in the restart of stalled replication forks, during which the proteins, DnaT, PriA, PriB and PriC, are of great significance. The replication restart proteins mediate the response to the dissociation of the replisome from the DNA template.

Genetic studies identifying the essentiality of primosomal proteins (PriA, PriB, PriC) indicate that conflict resolution by replication restart is a fundamental mechanism of DNA replication (Mangiameli et al., 2017). However, up to 20% of stalled forks may form collapsed forks, particularly in the event of collisions from subsequent replication forks. In the event of fork collapse, the structure must be reformed via recombination-mediated strand invasion (Michel et al., 2018). Therefore, the rapid and effective restart of replication forks is essential for cell survival, highlighting the continuous need for replication restart proteins even in wild-type cells.

Rather than assembling at a specific DNA sequence, as is the case for replication initiation at oriC, replication is restarted at specific structures (Sandler et al., 2021). The restart primosomal proteins use recombination intermediates and stalled replication forks as substrates to load new replication forks via different pathways. PriA is required for homologous recombination and double-strand break (DSB) repair, as well as the restart of stalled forks in coordination with PriC. PriB interacts with ssDNA in order to promote the helicase activity of PriA and DnaT is necessary for replisome reloading. At the centre of replication restart is the reloading of DnaB to facilitate the association of DnaG, the clamp loader and the core polymerase with the repaired fork.

Replication restart has been categorised into three distinct pathways considered to act on specific substrates, each mediated by a combination of the restart primosomal proteins. The most common mechanism for restart is thought to be the PriA/PriB pathway, given the relative severity of null mutations of each protein. Specifically, the deletion of PriA has been found to be detrimental to cell viability (McCool and Sandler, 2001), whilst PriB and PriC null-mutants do not exhibit a significantly altered phenotype when the remaining background is wild type, unless present as a double mutant (Sandler et al., 1999). Interestingly, the intrinsic activity of DnaT has yet to be well characterised. Despite this, DnaT is known to be essential in the replication restart pathway, with the deletion mutant displaying a similar phenotype to that of PriA null mutants (McCool et al., 2004).

In the main pathway, PriA recognises abandoned replication forks. The six domains of PriA act in cooperation to selectively bind forks. This interaction has a strong affinity and initiates the

docking of PriB to the PriA-replication fork complex. Recent biochemical and genetic studies have demonstrated a switch-like mechanism coupling fork recognition and formation of the PriA-PriB complex (Duckworth et al., 2023). This is followed by the recruitment of DnaT, forming a complex for the loading of DnaB onto the DNA template (Fujiyama et al., 2014). The remaining two pathways are PriA-PriC and PriC only. *In vitro* studies have shown that PriC is able to independently restart stalled replication forks via binding with ssDNA (Heller and Marians, 2005). However, the viability of PriC null mutants suggests that this is not a crucial pathway *in vivo*.

Aims and experimental design

This project aimed to use single-molecule fluorescence microscopy to analyse the dynamics of the replisome as it encounters an obstacle to replication. The initial hypothesis surrounds the 'traffic jam' model of the replication block. A single *E. coli* genome replication round can be completed in approximately 40 minutes. However, this must be achieved around 20 minutes before cell division. Since doubling times may be as quick as 20 minutes, cells must carry out multiple rounds of replication simultaneously (Den Blaauwen et al., 1999). Therefore, the 'traffic jam' refers to replisomes stacked up at the site of the block due to successive rounds of replication initiation. Importantly, by studying the $Lac0_{34}$ array in the context of cells with wild-type replication and repair machinery, this project provides a basis for future work which can explore differences in severity of the same obstacle under genetic perturbations.

In order to achieve this goal, a number of existing strains were imaged, and new strains were constructed with fluorescently tagged replisome components. A previous study investigating transcription factor-DNA complexes as blocks to replication in *E. coli* presented artificial arrays of LacO operators as a proxy for stalled arrays of RNA polymerase (Payne et al., 2006). The binding of the Lac repressor (LacI) to the operators creates a block to the replication fork. This method of artificial replication block allows the precise detection of the locus. It thus facilitates experiments to elucidate the molecular events that take place as the replisome encounters the block. Strains included in this study contained an artificial array of

34 lac operators engineered onto the chromosome (figure 4). Payne et al. (2006) demonstrated differences in the severity of the *lacO*$_{34}$ construct between in vitro and in vivo experiments. Cells were able to tolerate 34 tandem repeats of the lac operator and remain viable despite this blocking all forks in vitro. Since the cells with *lacO*$_{34}$ array are at the cusp of viability, with no observable wild type growth defects but serve defects in mutants, this thesis sets a baseline to explore replication block under further genetic perturbations such as deletions of restart proteins.

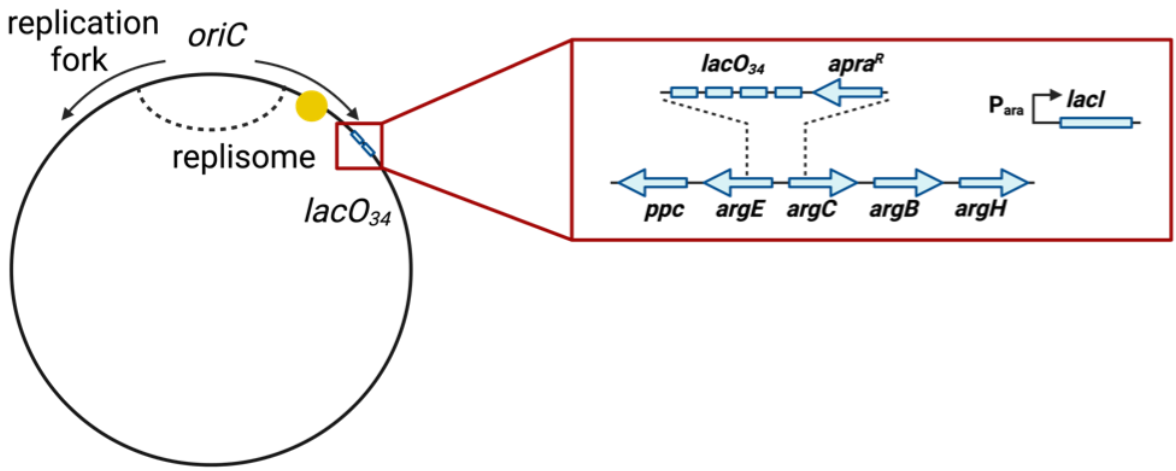

Figure 4. Lac operator array on E. coli chromosome. Addition of arabinose to culture media induces LacI which binds to LacO forming a complex that blocks replisome progression.

Cell cycles were synchronised across cultures due to a temperature-sensitive mutation in *dnaC*, which prevents replication initiation at 42°C. In wild type cultures, DnaC is necessary for the binding of DnaB to the origin and promotes the transition from initiation to elongation. Therefore, incubation for 90 minutes at 42℃ allows all current rounds of replication to be completed but no further rounds to start. Consequently, we were able to image the cultures for 100 minutes with replication initiated following a downshift in temperature, allowing for only a small percentage of cells to have replisomes potentially already stalled by the block. The synchronisation of the cultures and induction of the lac repressor formed the basis for the key experimental approaches.

The majority of results in this study were generated via slimfield microscopy (Plank et al., 2009) experiments to allow the detection of the replisome and *lac* operator array. Slimfield microscopy has emerged as a transformative approach enabling the study of the replisome at the level of single molecules. This method differs from standard epifluorescence microscopy in that the fluorescence excitation is limited to a narrow field comprising individual cells. Therefore, the excitation intensity is increased up to 1000-fold, increasing the signal to noise ratio and facilitating the imaging of single proteins at the millisecond timescale. Consequently, slimfield imaging is a key approach to the study of dynamics at the replication fork, where the diffusional motion of proteins occurs at such timescales.

Microscopy images were analysed to determine the colocalisation of the replisome and the lac operator array by monitoring the cell cycle at 10-minute intervals. This was complemented by flow cytometry to explore the progression of DNA replication in cells exposed to the block. In addition, growth curves were generated for all strains used in the project to confirm the validity of fluorescently tagged strains and to compare the viability of cultures expressing the lac repressor and those with the empty vector.

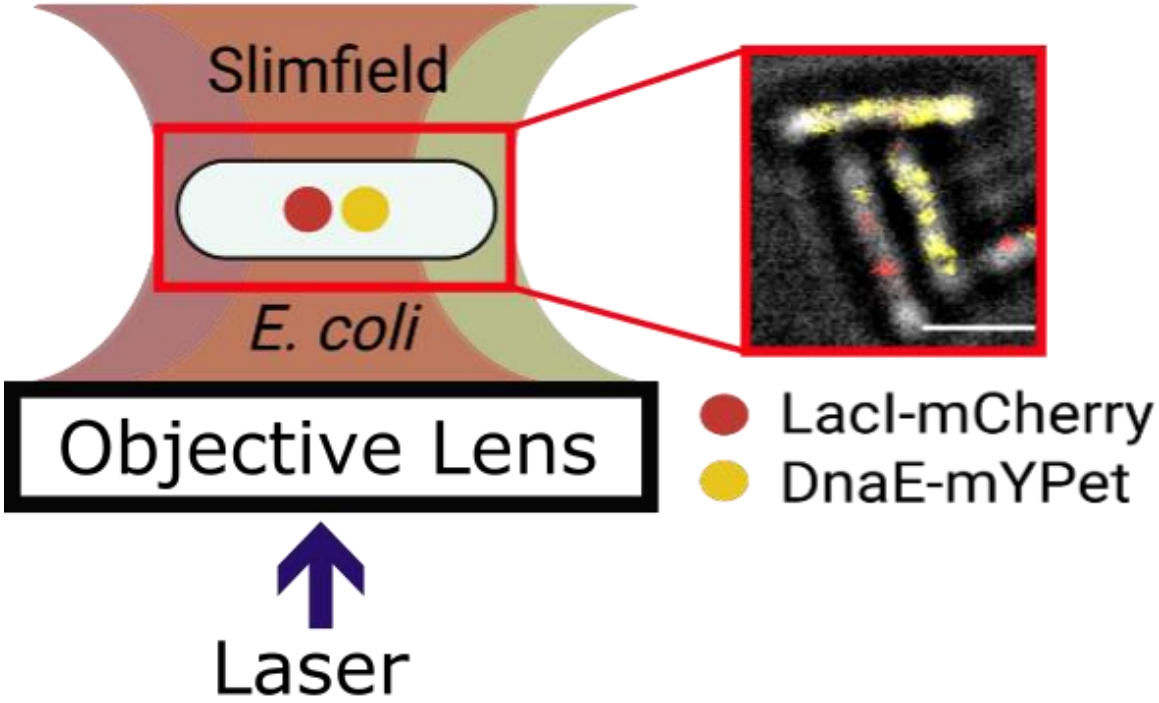

Figure 5. Slimfield microscopy: Millisecond timescale single-molecule detection. Fluorescence excitation limited to narrow, single cell fields. Representative Slimfield image with LacI-mCherry and DnaE-mYPet signal. Scale bar = 2µm. Adapted from (Wollman et al., 2021).

This study finds that approximately 20% of cells form *lac* repressor foci, which indicates the formation of repressor-operator complexes across the $LacO_{34}$ array. In addition, only 3% of cells demonstrated signals corresponding to replisome-repressor colocalisation. Consequently, these results suggest that the vast majority of wild-type *E. coli* cells are able to overcome the block either through cellular mechanisms acting to remove obstacles, the inefficacy of the block to prevent replisome progression, or efficient replication restart in the event of replisome stalling.

Further analysis of both the blocked and unblocked populations revealed that the stoichiometry of the repressor is increased when colocalised to the block, pointing to more severe conflicts preventing replisome translocation. In addition, exposure to the lac repressor reduces the overall replisome stoichiometry of the cells. The low level of replication conflict was substantiated by growth curves and flow cytometry, which showed little difference between repressor and control strains. In addition, single-molecule analysis of DnaT highlights

the role of replication restart as an essential mechanism to overcome more persistent blocks. Most significantly, the findings of this study support the 'traffic jam' model of replication block, with an increased stoichiometry of the replisome components colocalised to the block across the time course.

Methods

Strains and strain construction

Table 1. List of strains used in the project

Strain name	**Genotype**
AS467	*<kan>-mGFP-dnaT*
AS972	*leuB+ thr::Tn10dtet dnaC7 thr+ tetS*
AS985	*$lacO_{34}$ dnaC7 / pBAD24*
AS986	*$lacO_{34}$ dnaC7 /placI-mCherry*
AS993	*dnaQ-mYPet $lacO_{34}$ dnaC7*

AS996	*dnaQ-mYPet $lacO_{34}$ dnaC7 /placI-mCherry*
AS997	*dnaE-mYPet $lacO_{34}$ dnaC7*
AS1000	*dnaE-mYPet $lacO_{34}$ dnaC7 /placI-mCherry*
RH23	*<kan>-mGFP-dnaT $lacO_{34}$ dnaC7 /placI-mCherry*
RH25	*<kan>-mGFP-dnaT $lacO_{34}$ dnaC7*
RH28	*$lacO_{34}$ dnaC7 /placI*

List of Plasmids

Table 2. List of plasmids used in the project

Plasmid name	**Genotype**
pBAD24	*Plasmid containing an arabinose-inducible promoter*
pPM306	*pBAD-lacI*
pAS17	*pBAD24-lacImCherry*

Frozen stocks were revived on LB plates containing 20uM ampicillin and 0.5mM IPTG at 30℃ then inoculated in liquid LB with ampicillin and IPTG and grown overnight at 30℃.

DnaT-GFP strain construction:

A P1 lysate was generated for the *<kan>-mGFP-dnaT* construct from the strain AS467. 10µL of 0.5M $CaCl_2$ and 10^7 pfu of stock P1 lysate was added to 300µL of overnight AS467 culture. The culture was incubated at 37℃ for 15 minutes to allow adsorption and then diluted in 10mL LB with 100µL 0.5M $CaCl_2$. The diluted culture was incubated at 37℃ with 180 rpm shaking until visible lysis of the culture. 300 µL of CHCl3 was added, followed by shaking for 10 minutes and centrifugation at 4000 RPM for 10 minutes. The supernatant was transferred to a fresh tube with 1mL chloroform and stored at 4℃.

To transduce the *<kan>-mGFP-dnaT* construct into strains AS986 and AS985, a 1mL volume of overnight AS986 and AS985 cultures was treated with 10µL 0.5M $CaCl_2$ and 100µL lysate. The culture was incubated for 15 minutes at 30℃, then centrifuged at 6000 RPM for 5 minutes and resuspended in 1mL LB with 20 mM sodium citrate. A second incubation was conducted at 30℃ for 30 minutes without shaking, followed by centrifugation and resuspension in 100µL LB with 10µL 1M sodium citrate. The final culture was plated on LB with kanamycin. The strain was selected for growth on kanamycin and verified by PCR using primers OJGB437 and OJGB439.

Untagged LacI plasmid strain construction

A competent AS972 culture was prepared by growing to the mid-log phase and then centrifuged for 5 minutes at 6000 rpm. The pellet was resuspended in chilled 0.1M $CaCl_2$ and centrifuged again for 5 minutes at 6000 rpm before resuspension in 0.1M $CaCl_2$ and incubated on ice for 30 minutes. 100 ng of plasmid DNA (pPM306) was added to 100ul of competent cells and incubated on ice for 30 minutes. The cells were subjected to heat shock by incubating at 42℃ for 90 seconds and then stored on ice for one minute. 1mL of LB media was added, and the culture was incubated for 40 minutes at 30℃, then centrifuged (6000 rpm for 5 minutes) and resuspended in 100 µL LB. Cells were plated on LB with ampicillin and IPTG and grown overnight at 30℃.

Growth curves

Cultures were grown in minimal media (M9 with the following supplements: glycerol, MgSO4, CaCl2, B1, arginine, IPTG, and ampicillin) with IPTG and ampicillin overnight and then washed twice to remove IPTG. Cultures were then diluted 1:10 in minimal media and treated with arabinose to induce the lac repressor. 100 µL aliquots of the diluted cultures were pipetted into separate wells of a 96-well clear flat bottom sterile microplate. Minimal media containing arabinose was used as a blank for the experiment. Growth curves were carried out using a SPECTROstar Nano plate reader at 30℃ over the course of 18 hours. The optical density (OD6000) values were recorded across the time series, and the doubling time was calculated as the time taken for a 2-fold increase in OD_{600} throughout the exponential growth phase. Three replicates of each strain were grown for reproducibility.

Microscopy and image analysis

Cultures were diluted 1:50 and incubated for 24 hours at 30℃ to mid-log phase in 10 mL minimal media (M9 with the following supplements: glycerol, MgSO4, CaCl2, B1, arginine, IPTG, and ampicillin). After growth to mid-log phase, cultures were washed twice of IPTG by centrifuging 1 mL of culture and resuspending in M9 with glycerol, MgSO4, CaCl2, B1, arginine, and ampicillin. 990 µL of supernatant was discarded, with the pellet resuspended in the remaining supernatant.

Microscope slides were prepared with an overlay of M9, 0.2% arabinose and 1% agarose. Cultures were spotted onto the slide and sealed with a plasma-cleaned coverslip, then immediately placed in the temperature-controlled microscope chamber preheated to 42℃. Slides were incubated at 42℃ for 90 minutes. After 90 minutes, the temperature-controlled chamber was reduced to 30℃, and the slide was imaged immediately for 100 minutes. This includes the first 10 minutes for the chamber to reach 30℃..

Imaging was carried out using a bespoke dual-colour single-molecule microscope with excitation from a 514 nm and 561 nm, 50 mW Obis laser (ran at 20 mW and 40 mW, respectively). This was coupled into a Zeiss microscope body with a Mad City Lab's nano stage.

Slimfield illumination was achieved by narrowing the lasers to 10 µm at full half width maximum in the sample plane.

Alternative excitation with a 5 ms exposure time was generated by digital modulation of the lasers using the National Instruments dynamic I/O module NI 9402. Yellow/red images were split using a bespoke colour splitter comprising a dual-pass yellow/red dichroic mirror centred at longpass wavelength (561 nm). Emission filters for yellow and red were centred at 535 nm and 610 nm respectively.

For DnaT imaging, splitting of green/red images was performed using a bespoke colour splitter comprising a dual-pass green/red dichroic mirror centred at 561 nm. Emission filters for green and red were centred at 525 nm and 610 nm respectively.

Data analysis

Slimfield images were analysed using custom ADEMscode software in MATLAB, which automatically detects and tracks foci (Miller et al., 2015). Foci were accepted if the signal-to-noise ratio (SNR) of 0.4 was less than the intensity of the foci. Foci were determined to be in linked trajectories if they were within five pixels and persisted for a minimum of four image frames consecutively. The intensity of a single mYPet or mCherry protein was determined using ADEMscode to calculate the stepwise photobleaching of proteins over 1000 frames. This allowed the calculation of the stoichiometry of the replisome proteins and LacI by dividing the intensity of the detected foci by the intensity of a single mYPet or mCherry protein. The number of foci in each cell was determined using the number of trajectories of each fluorescent protein, and the cell size was calculated from cell area data generated by the MATLAB code.

Flow cytometry

Strain preparation

Strains AS985 and RH28 were grown to mid-log phase at 30℃ in minimal media (M9 with the following supplements: glycerol, $MgSO_4$, $CaCl_2$, B1, arginine, IPTG and ampicillin). The tubes were transferred to a 42℃ incubator for 90 minutes, with arabinose added at the 60-minute time point to induce the lac repressor. At 90 minutes, 100µL samples were taken for each strain and treated with 1µL of 1.5 mg/ml cephalexin to prevent cell division. 5mL of minimal media containing arabinose pre-chilled to 18℃ was added to the culture, followed by immediate incubation at 30. Every 10 minutes after the temperature shift to 30℃, 200µL samples were taken, treated with 2µL of 1.5 mg/mL cephalexin, and incubated at 42℃ for 90 minutes. Processing of samples following incubation at 42℃ involved centrifugation at 13000 RPM for 1 minute and resuspension in 100µL PBS. Final samples were treated with 400 µL of 100% methanol, then vortexed and stored at -20 C.

Staining

Staining was carried out using SYTOX ® Green and RNase A made up in PBS at the following concentrations: 1µM SYTOX ® Green and 50 µg/ml RNase A. Samples were washed of methanol by centrifuging for 1 minute at 13000 RPM, followed by resuspension in 500 µL PBS. They were centrifuged a second time, resuspended in SYTOX mix, and stored in the dark at 4℃ overnight.

Flow cytometry protocol and analysis

Flow cytometry experiments were carried out on the CytoFLEX LX375/355. DNA-bound SYTOX green has a maximal absorption of 502 nm and a maximal emission of 523 nm. Therefore, the fluorophore can be excited by a 450-490 nm source. A minimum of 50,000 events were recorded for each of the three technical replicates per sample. Analysis was carried out using the CytExpert software. Events were gated based on the peaks at one and two chromosome copies, with an additional gate representing the region between the two peaks. The

percentage of events for samples in each gate was determined, and differences between time points were determined based on standard error.

Results

21% of cells form lac repressor-operator complexes with a maximum stoichiometry of 24

Temperature-sensitive cultures were grown to mid-log phase in minimal media at 30℃, then spotted onto a microscope slide with an overlay consisting of minimal media and agarose treated with arabinose to induce the lac repressor. Slides were incubated at 42℃ in order to synchronise the cultures and allow the formation of lac repressor-operator complexes. After 90 minutes, the temperature-controlled microscope chamber was reduced to 30℃, and imaging was carried out for 100 minutes.

The lac repressor was tagged with mCherry to allow visualisation with single-molecule detection using slimfield microscopy. Of all cells detected, 20.9±0.01% (mean ± standard error) (DnaE) (n = 5310) and 24.8±0.01% (DnaQ) (n = 4389) had LacI-mCherry foci. The majority of cells with a signal had only one focus, making up 14.1±0.01% (DnaE) and 18.5±0.01% (DnaQ) of all cells, with a minority of cells having two (4.7±0.003% - DnaE and 4.9±0.003% - DnaQ) or more foci (2.1±0.002% - DnaE and 1.1±0.002% - DnaQ). Conversely, 79.2±0.01% had no LacI-mCherry signal in the DnaE tagged strain, and 75.2±0.01% had no LacI-mCherry signal in the DnaQ tagged strain.

The mean total LacI stoichiometry for cells in which LacI-mCherry signal was detected was quantified to be 3.7±0.7 for the DnaE-mYPet strain (figure 6) and 4.2±0.1 for the DnaQ-mYPet strain (figure 7). Dunnett's tests demonstrated that the stoichiometry of the total LacI signal in the DnaE strain increases significantly from an average of 3.2±0.2 during the first time point, during which the temperature is downshifted, to 4.2±0.2 at the 20-30 minute interval ($p=0.01$).

Similarly, between 60 and 80 minutes, there is a significant increase compared to the initial time point, with values reaching 4.3±0.2 ($p= 0.002$) and 4.5±0.3 ($p= 0.0003$). The DnaQ tagged strain also demonstrates significant changes in stoichiometry over time, with an initial value

of 4.7±0.3 decreasing between 10 and 30 minutes to 2.6±0.1 (p= 0.0002) and 3.2±0.2 (p= 0.02). This is followed by an increase at 60-70 minutes to 6.2±0.6 (p = 0.005) and an eventual decrease at the 80-90 minutes period with a stoichiometry of 2.6±0.1 (p= 0.0003).

Additionally, the maximum occupancy of the array was calculated from the maximum stoichiometry values across all time points, with a result of 23.8. Furthermore, observations from a sample size of 127 tracks of LacI-mCherry signal indicated a periodicity of four (figure 8), consistent with the oligomeric state of LacI as a tetramer. However, it should be noted that the first peak is at approximately two, suggesting the fundamental subunit is a dimer. This indicates that the maximum occupancy of the lac operator in these experiments is equivalent to six tetramers. In addition, the copy number of LacI-mCherry was determined using custom matlab scripts. Three of the AS1000 replicates were analysed, resulting in copy number and standard error of 86.19±3.9, 43.52±1.4 and 40.15±1.2, with a standard deviation of 25.7. This suggests that LacI-mCherry is not expressed at a level which could meet the occupancy of the entire 34 operator array, which would correspond to 136 molecules (34 times the tetrameric state of LacI).

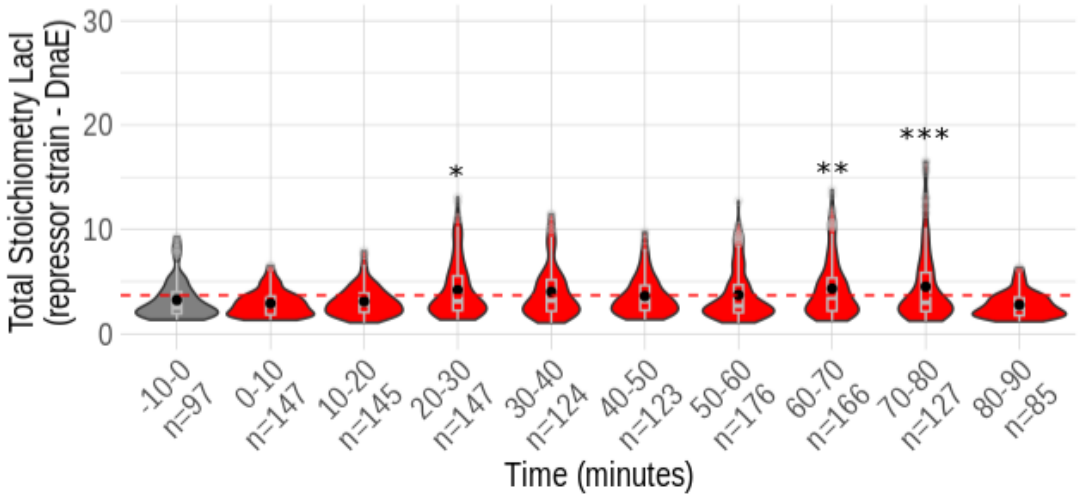

Figure 6. LacI total stoichiometry AS1000 (DnaE-mYPet) with LacI-mCherry induced. First time point represents the temperature downshift period. Red dotted line represents the mean stoichiometry

*across all time points. Boxplots show median and interquartile range and black dots on graphs show means. (Mean and standard errors values: 3.2±0.2, 2.9±0.1, 3.1±0.1, 4.2±0.2, 4.03±0.2, 3.6±0.2, 3.7±0.2, 4.3±0.2, 4.5±0.3, 2.8±0.1). Dunnett's tests were performed comparing all time points to the -10-0 minute interval, significant changes ($p < 0.05$) in stoichiometry are as follows: 20-30 ($p = 0.01$), 60-70 ($p = 0.002$), 70-80 ($p = 0.0003$). Stars show significant results ($p < 0.001$ '***', $p < 0.01$ '**', $p < 0.05$ '*').*

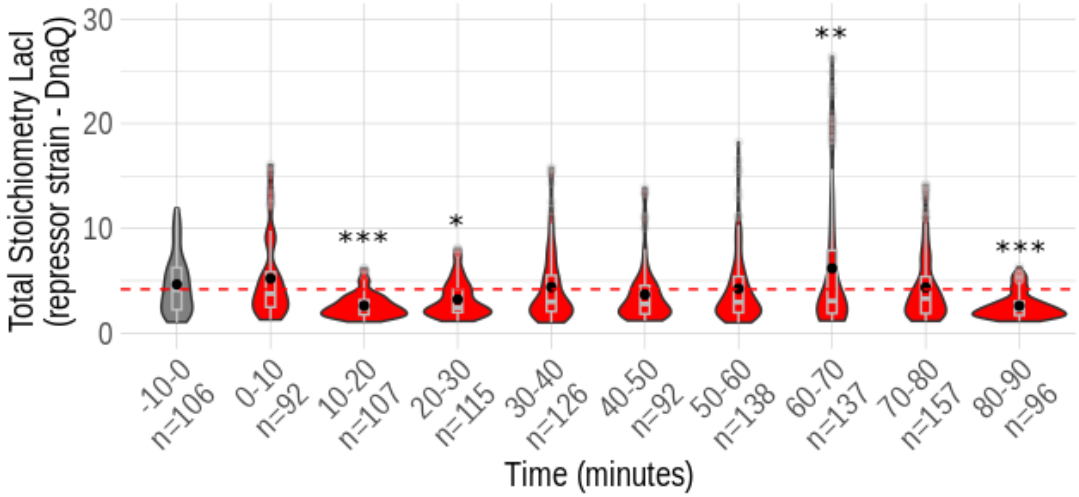

*Figure 7. LacI total stoichiometry AS996 (DnaQ-mYPet) with LacI-mCherry induced. First time point represents the temperature downshift period. Red dotted line represents the mean stoichiometry across all time points. Boxplots show median and interquartile range and black dots on graphs show means. (Mean and standard errors values: 4.7±0.3, 5.2±0.4, 2.6±0.1, 3.2±0.2, 4.4±0.3, 3.7±0.3, 4.2±0.3, 6.2±0.6, 4.4±0.3, 2.6±0.1). Dunnett's tests were performed comparing all time points to the -10-0 minute interval, significant changes ($p < 0.05$) in stoichiometry are as follows: 10-20 ($p = 0.0002$), 20-30 ($p = 0.02$), 60-70 ($p = 0.005$), 80-90 ($p = 0.0003$). Stars show significant results ($p < 0.001$ '***', $p < 0.01$ '**', $p < 0.05$ '*').*

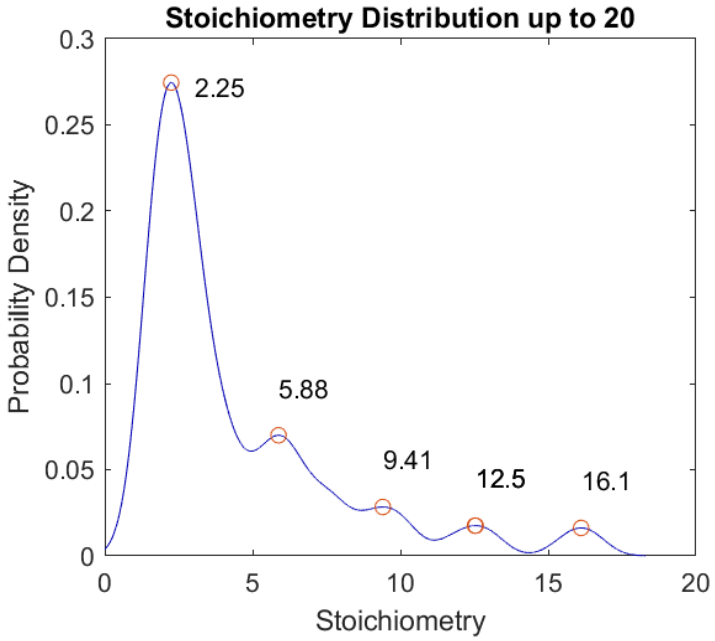

Figure 8. LacI-mCherry periodicity distribution plot. Number of tracks = 127. Periodicity indicates the oligomeric state of the protein. Approximate periodicity of four indicates LacI is tetrameric.

The percentage of cells with DnaE or DnaQ foci is decreased following lac repressor expression

To investigate the localisation of the replisome components DnaE and DnaQ in relation to the lac operator-repressor complexes, fluorescent fusions of the proteins labelled with mYPet were introduced to the strains containing LacI-mCherry. These strains were imaged using dual colour Slimfield microscopy to detect single molecules as well as colocalisation between the replisome proteins and binding of the lac repressor to the array.

Analysis of the microscopy images revealed the strain on its own and not expressing lacI showed DnaE signal in 71.4±0.01% of cells (n = 1593) (figure 9), with 28.6±0.01% having no foci, 35.4±0.01% having one focus, 23.7±0.01% having two foci and 12.4±0.01% having three or more foci. In addition, analysis of DnaQ imaging experiments revealed the DnaQ strain not expressing lacI demonstrated mYPet signal at a rate of 61.4±0.01% of all cells (n = 1436). This corresponds to 36±0.01% with one focus, 18±0.01% with two foci, 7.4±0.01% with three or more foci, and 38.7±0.01% with no foci. In comparison, 56.2±0.01% of all cells (n = 4158) expressing the lac repressor had signal corresponding to DnaE-mYPet (figure 10). The majority of cells with signal had one focus (35.4±0.01% of all cells). Of the remaining cells, 16.2±0.01% had two foci, 4.6±0.01% had three or more foci and 43.8±0.00% had no foci. Similarly, 49.7±0.01% of all repressor expressing cells (n = 4389) had signal corresponding to DnaQ-mYPet. The majority of cells with signal had one focus (35.9±0.01% of all cells). Of the remaining cells 11.6±0.01% had two foci, 2.2±0.002% had three or more foci and 50.3±0.01% had no foci.

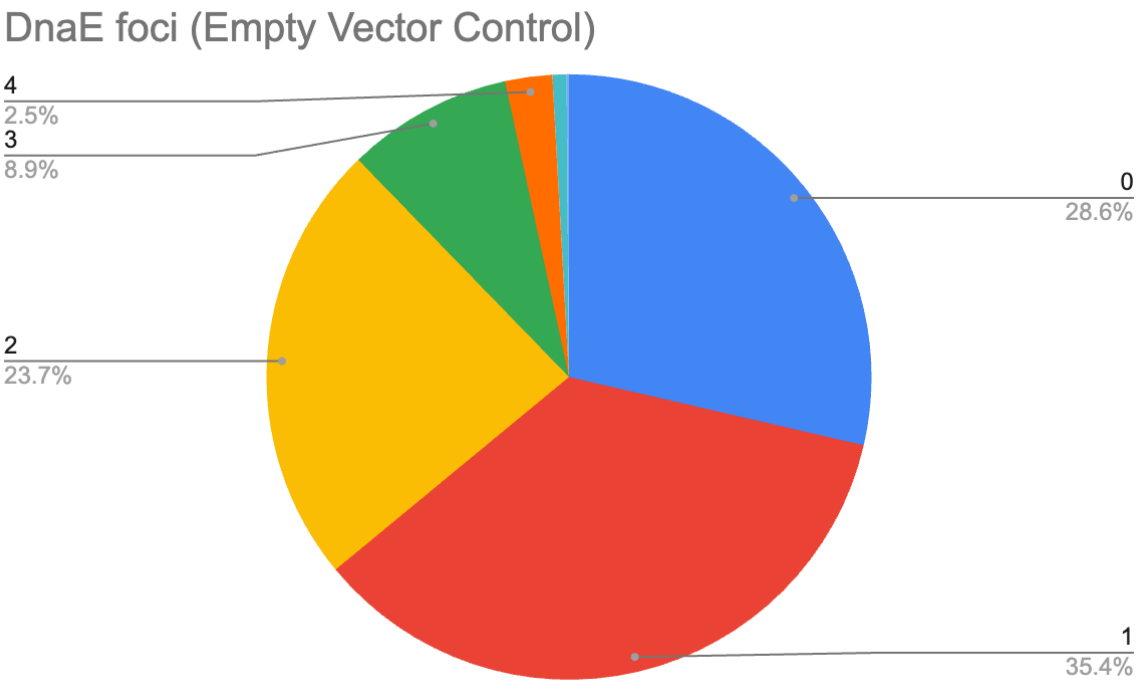

Figure 9. Percentage of cells with different numbers of foci. Plot for strain AS997 (empty vector). Percentage and standard error for each section (standard deviation between experiments in brackets): 0 foci = 28.6±0.01 (±2.12), 1 focus = 35.4±0.01 (±2.03) , 2 foci = 23.7±0.01 (±1.39), 3 foci = 8.9±0.00 (±1.07) , 4+ foci = 3.6±0.01 (±0.23). Data from two repeats, total number of cells analysed = 1593.

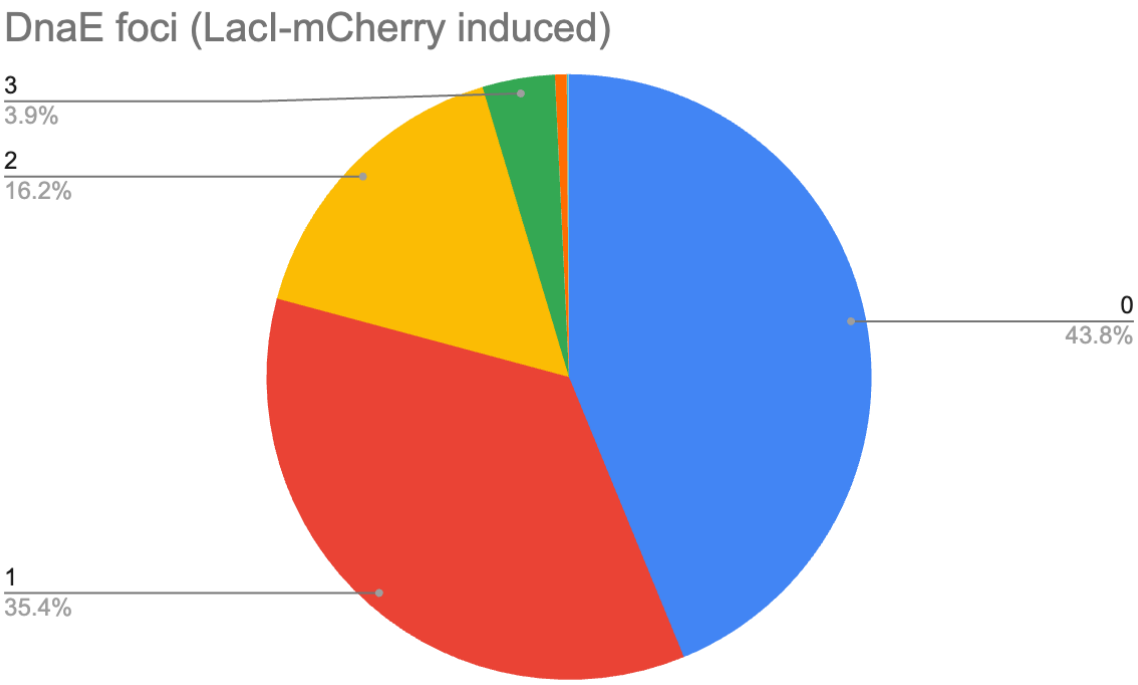

Figure 10. Percentage of cells with different numbers of foci. Plot for strain AS1000 (lac repressor). Percentage and standard error for each section (standard deviation between experiments in brackets): 0 foci = 43.8±0.01 (±13.4), 1 focus = 35.4±0.01 (±6) , 2 foci = 16.2±0.01 (±5.37), 3 foci = 3.9±0.00 (±1.93). Data from four repeats, total number of cells analysed = 4158.

Mean stoichiometries of total replisome components are consistent over the time course, but reduced in cultures expressing the lac repressor.

Strains containing the replisome protein fluorescent fusions with an empty plasmid lacking LacI-mCherry, and therefore unable to create the repressor-operator complexes upon addition of arabinose, were imaged in the same conditions over the same time course.

The mean total stoichiometry for DnaE in the repressor strain (figure 11) shows an initial increase from the -10-0 minutes time period during which the temperature downshift occurs, starting at 6.7±0.2. This increases significantly by 0-10 minutes to 7.9±0.2 ($p = 0.002$), with all subsequent time points demonstrating a significant increase compared to the initial value, peaking at 80-90 minutes with a value of 8.5±0.3 ($p= 2.9e-06$). This could be attributed to replication initiation occurring at the permissive temperature.

These results are similar to the pattern of DnaQ repressor strain stoichiometry increase (figure 12). The initial value at -10-0 minutes is a stoichiometry of 5.2±0.2. However, there is no significant increase until the 20-30 minute time interval (6.2±0.2, $p= 0.003$), which also represents the highest value for stoichiometry of the time series. The stoichiometry remains significantly higher from that of the first time interval until 60-70 minutes, when it decreases to a value of 5.6±0.2 and shows no significant difference for the remaining time intervals.

Both the repressor and control strains demonstrated the same increase following the temperature downshift. However, the mean stoichiometry over the time course is increased in the control strains (10.9±0.2 - DnaE (figure 13) and 9.4±0.2 - DnaQ (figure 14)) compared to strains with the Lac repressor induced for both the linked and total replisome stoichiometry. Finally, observations from a sample size of 278 tracks of DnaE-mYPet signal indicated a periodicity of three (figure 15), consistent with the oligomeric state of DnaE as a trimer.

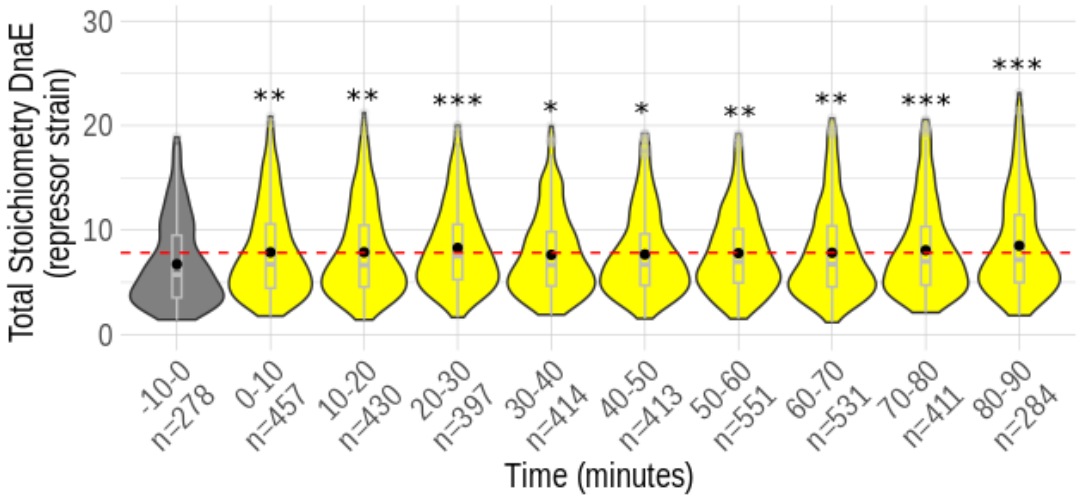

*Figure 11. DnaE total stoichiometry AS1000 (DnaE-mYPet, lacI-mCherry). First time point represents the temperature downshift period. Red dotted line represents the mean stoichiometry across all time points. Boxplots show median and interquartile range and black dots on graphs show means. (Mean and standard errors values: 6.7±0.2, 7.9±0.2, 7.9±0.2, 8.3±0.2, 7.6±0.2, 7.7±0.2, 7.8±0.2, 7.8±0.2, 8.1±0.2, 8.5±0.3). Dunnett's tests were performed comparing all time points to the -10-0 minute interval, significant changes ($p < 0.05$) in stoichiometry are as follows: 0-10 ($p = 0.002$), 10-20 ($p = 0.003$), 20-30 ($p = 1.1e-05$), 30-40 ($p = 0.03$), 40-50 ($p = 0.02$), 50-60 ($p = 0.004$), 60-70 ($p = 0.003$), 70-80 ($p = 0.0003$), 80-90 ($p = 2.9e-06$). Stars show significant results ($p < 0.001$ '***', $p < 0.01$ '**', $p < 0.05$ '*').*

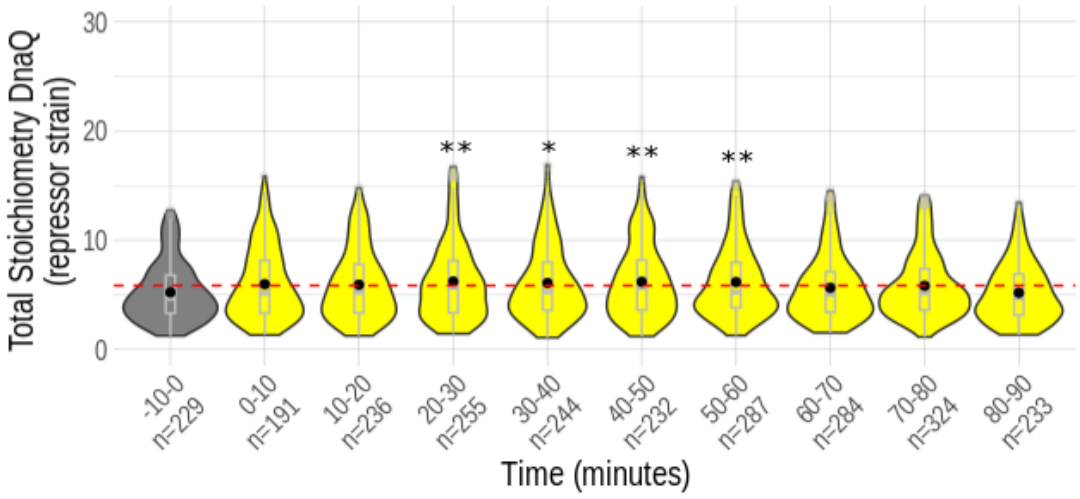

*Figure 12. DnaQ total stoichiometry AS996 (DnaQ-mYPet, lacI-mCherry). First time point represents the temperature downshift period. Red dotted line represents the mean stoichiometry across all time points. Boxplots show median and interquartile range and black dots on graphs show means. (Mean and standard errors values: 5.2±0.2, 6±0.2, 5.9±0.2, 6.2±0.2, 6.1±0.2, 6.2±0.2, 6.2±0.2, 5.7±0.2, 5.8±0.2, 5.2±0.2). Dunnett's tests were performed comparing all time points to the -10-0 minute interval, significant changes ($p < 0.05$) in stoichiometry are as follows: 20-30 ($p = 0.003$), 30-40 ($p = 0.02$), 40-50 ($p = 0.007$), 50-60 ($p = 0.005$). Stars show significant results ($p < 0.001$ '***', $p < 0.01$ '**', $p < 0.05$ '*').*

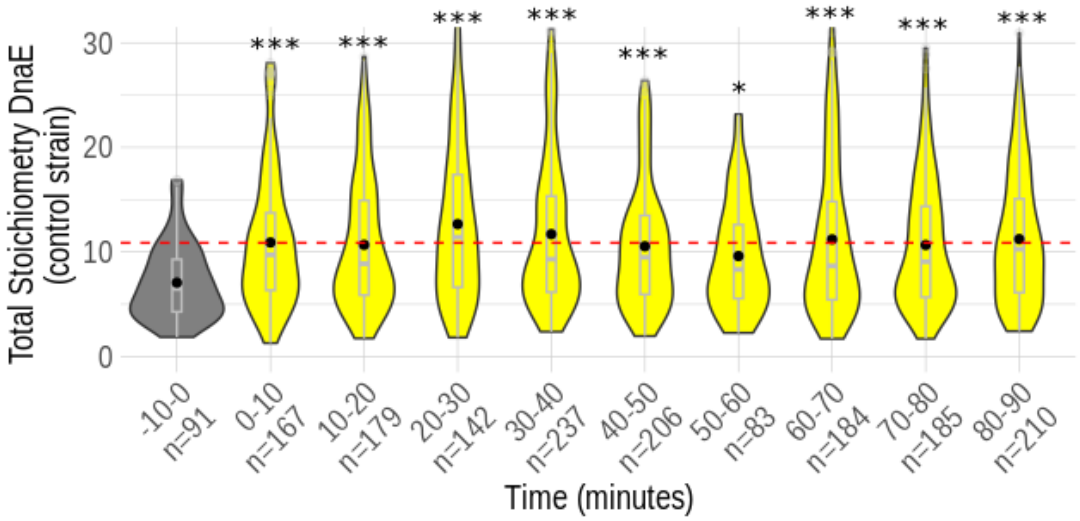

*Figure 13. DnaE total stoichiometry AS997 (DnaE-mYPet, empty vector). First time point represents the temperature downshift period. Red dotted line represents the mean stoichiometry across all time points. Boxplots show median and interquartile range and black dots on graphs show means. (Mean and standard errors values: 7.1±0.4, 10.9±0.5, 10.7±0.5, 12.7±0.6, 11.7±0.5, 10.5±0.4, 9.6±0.6, 11.2±0.5, 10.7±0.5, 11.2±0.4). Dunnett's tests were performed comparing all time points to the -10-0 minute interval, significant changes ($p < 0.05$) in stoichiometry are as follows: 0-10 ($p = 3.3e-05$), 10-20 ($p = 0.0001$), 20-30 ($p = 4.4e-10$), 30-40 ($p = 1.0e-07$), 40-50 ($p = 0.0001$), 50-60 ($p = 0.05$), 60-70 ($p = 3.0e-06$), 70-80 ($p = 0.0001$), 80-90 ($p = 7.9e-07$). Stars show significant results ($p < 0.001$ '***', $p < 0.01$ '**', $p < 0.05$ '*').*

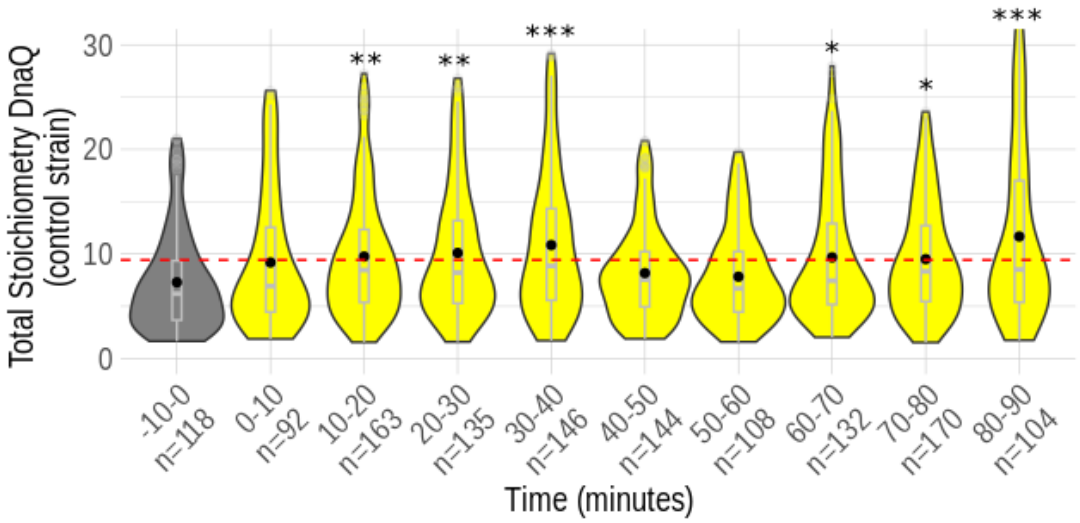

*Figure 14. DnaQ total stoichiometry AS993 (DnaQ-mYPet, empty vector). First time point represents the temperature downshift period. Red dotted line represents the mean stoichiometry across all time points. Boxplots show median and interquartile range and black dots on graphs show means. (Mean and standard errors values: 7.3±0.4, 9.2±0.7, 9.8±0.5, 10.1±0.5, 10.8±0.6, 8.2±0.4, 7.8±0.4, 9.7±0.5, 9.5±0.4, 11.7±0.8). Dunnett's tests were performed comparing all time points to the -10-0 minute interval, significant changes ($p < 0.05$) in stoichiometry are as follows: 10-20 ($p = 0.004$), 20-30 ($p = 0.001$), 30-40 ($p = 9.2e-06$), 60-70 ($p = 0.01$), 70-80 ($p = 0.01$), 80-90 ($p = 2.2e-07$). Stars show significant results ($p < 0.001$ '***', $p < 0.01$ '**', $p < 0.05$ '*').*

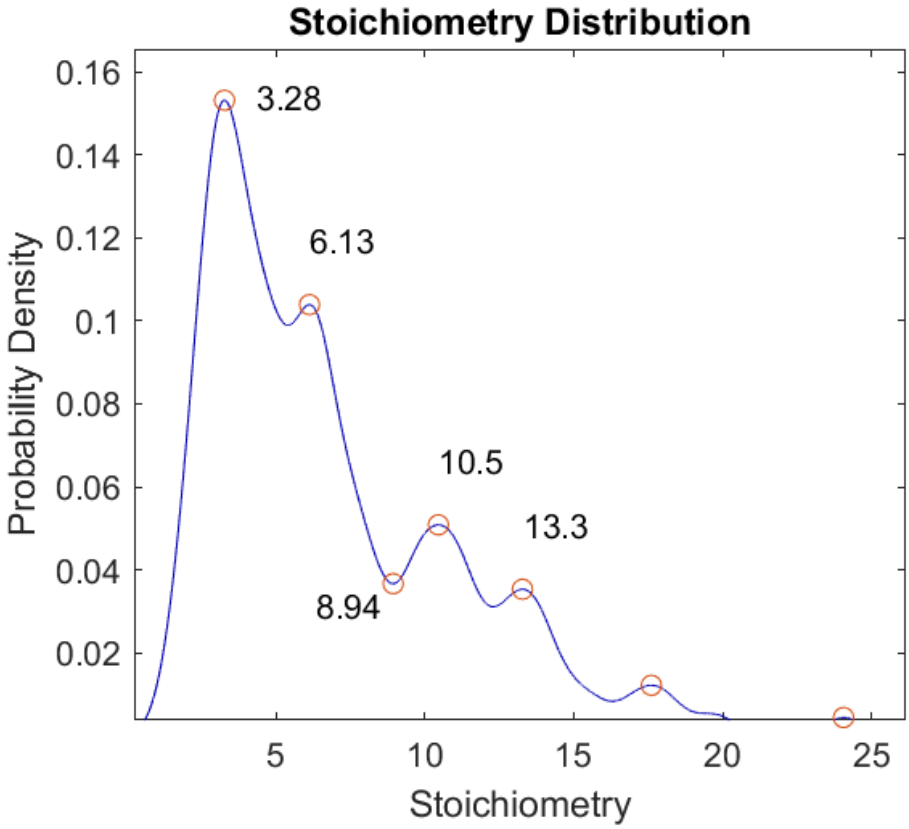

Figure 15. DnaE-mYpet periodicity distribution plot. Number of tracks = 278. Periodicity indicates the oligomeric state of the protein. Approximate periodicity of three indicates DnaE is trimeric.

The lac repressor-operator complexes block replisome foci in approximately 3% of cells, with DnaE and DnaQ stoichiometry increasing throughout the cell cycle.

In approximately 3% of cells expressing the lac repressor, both DnaE-mYPet and DnaQ-mYPet demonstrated a signal linked to LacI-mCherry. Prior to the temperature downshift, initial stoichiometry values at the first time point were 6.3±0.8 for DnaE and 4.4±0.7 for DnaQ. The mean stoichiometry undergoes a gradual increase from the 0-10 minute interval (9.8±1.2 and 5.9±0.67), reaching peaks of 12.7±1.8 and 10.2±1.2 at 50-60 and 60-70 minutes for DnaE (figure 16) and DnaQ (figure 17) respectively. This is followed by a decrease to 8.2±0.7 and 4.8±1.1 at the 80-90 minute time intervals.

However, only the peaks between 40 to 60 minutes (DnaE, p at 40-50 = 0.03, p at 50-60 = 0.008) and 60 to 80 minutes (DnaQ, p at 60-70 = 0.004, p at 70-80 = 0.02) represent significant increases compared to the values at the non-permissive temperature, with the following time points returning to a level of insignificance relative to the initial values. Notably, there is a time delay of approximately 20 minutes between the increase in DnaQ stoichiometry and the increase in DnaE stoichiometry, as well as the subsequent drop following these peaks.

In addition, both strains demonstrate a dip in mean stoichiometry early on in the cell cycle, before the peaks between 50 and 70 minutes. For DnaE, this occurs at the 10-20 minute period with a mean stoichiometry of 8.1±0.8 and for DnaQ at 30-40 minutes with a mean stoichiometry of 5.4±0.7. However, t-tests found that these stoichiometry dips at early time points were not significant (t = 1.2, df = 27.9, p-value = 0.2 and t = 0.8, df = 10, p-value = 0.4).

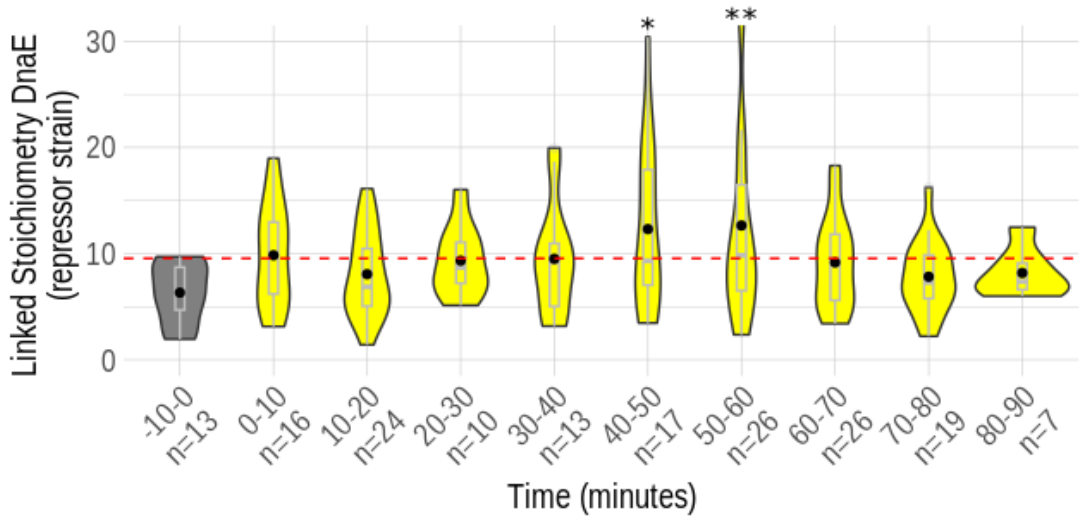

*Figure 16. DnaE linked stoichiometry AS1000 (DnaE-mYPet, lacI-mCherry). First time point represents the temperature downshift period. Red dotted line represents the mean stoichiometry across all time points. Boxplots show median and interquartile range and black dots on graphs show means. (Mean and standard errors values: 6.3±0.8, 9.8±1.2, 8.1±0.8, 9.3±1.1, 9.5±1.5, 12.3±1.9, 12.7±1.8, 9.2±0.9, 7.8±0.8, 8.2±0.9). Dunnett's tests were performed comparing all time points to the -10-0 minute interval, significant changes (p < 0.05) in stoichiometry are as follows: 40-50 (p = 0.03), 50-60 (p = 0.008). Stars show significant results (p < 0.001 '***', p < 0.01 '**', p < 0.05 '*').*

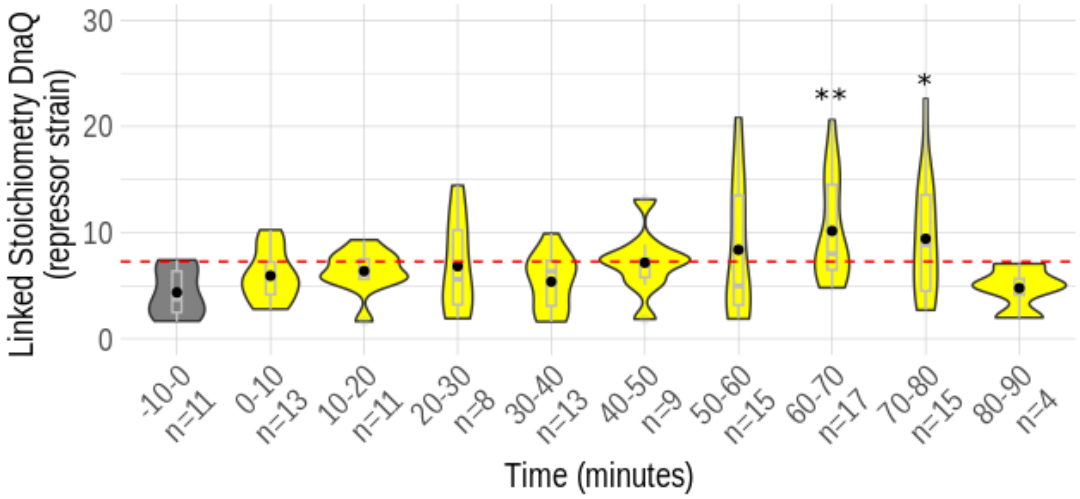

*Figure 17. DnaQ linked stoichiometry AS996 (DnaQ-mYPet, lacI-mCherry). First time point represents the temperature downshift period. Red dotted line represents the mean stoichiometry across all time points. Boxplots show median and interquartile range and black dots on graphs show means. (Mean and standard errors values: 4.4±0.7, 5.9±0.7, 6.4±0.6, 6.8±1.6, 5.4±0.7, 7.2±1.01, 8.4±1.6, 10.2±1.2, 9.4±1.4, 4.8±1.1). Dunnett's tests were performed comparing all time points to the -10-0 minute interval, significant changes ($p < 0.05$) in stoichiometry are as follows: 60-70 ($p = 0.004$), 70-80 ($p = 0.02$). Stars show significant results ($p < 0.001$ '***', $p < 0.01$ '**', $p < 0.05$ '*').*

Mean lac repressor stoichiometry is increased at sites of replisome block and remains stable over time.

The stoichiometry of LacI-mCherry colocalised to the replisome components was analysed (figures 18 and 19). Dunnett's tests demonstrated no significant differences between the mean stoichiometries at different time points, with overall time course means of 5±0.3 (DnaE) and 6.2±0.5 (DnaQ). However, this was found to be greater than the overall mean time course stoichiometry for total LacI-mCherry foci, with values of 3.7±0.07 (DnaE) and 4.2±0.1 (DnaQ).

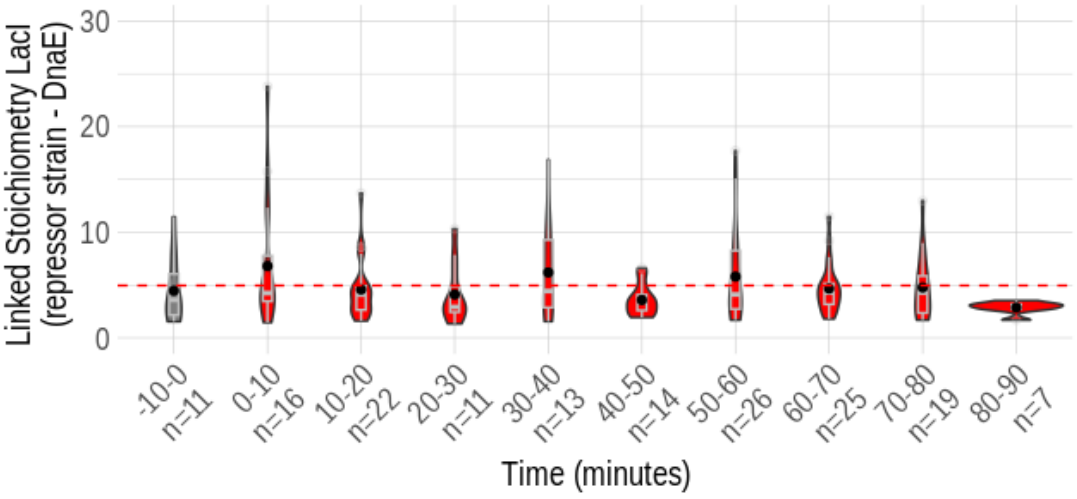

Figure 18. LacI linked stoichiometry AS1000 (DnaE-mYPet) with LacI-mCherry induced. First time point represents the temperature downshift period. Red dotted line represents the mean stoichiometry across all time points. Boxplots show median and interquartile range and black dots on graphs show means. (Mean and standard errors values: 4.5±1, 6.8±1.5, 4.6±0.6, 4.1±0.9, 6.2±1.3, 3.6±0.4, 5.8±0.9, 4.7±0.5, 4.8±0.7, 2.9±0.2). Dunnett's tests were performed comparing all time points to the -10-0 minute interval, with no significant changes found in stoichiometry over time at $p < 0.05$ significance level.

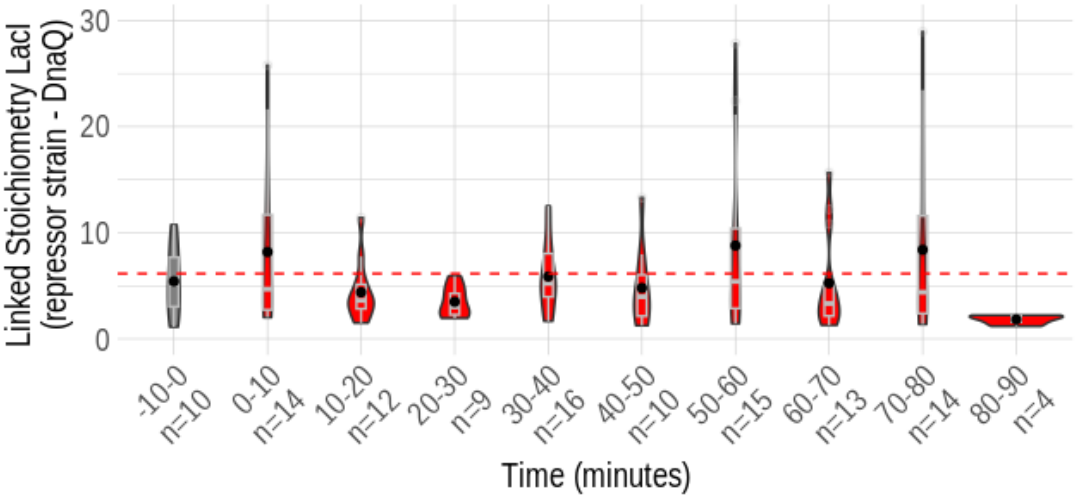

Figure 19. LacI linked stoichiometry AS996 (DnaQ-mYPet) with LacI-mCherry induced. First time point represents the temperature downshift period. Red dotted line represents the mean stoichiometry across all time points. Boxplots show median and interquartile range and black dots on graphs show means. (Mean and standard errors values: 5.4±1.03, 8.2±2.04, 4.4±0.8, 3.5±0.5, 5.9±0.8, 4.8±1.2, 8.8±2.2, 5.2±1.3, 8.4±2.4, 1.8±0.2). Dunnett's tests were performed comparing all time points to the -10-0 minute interval, with no significant changes found in stoichiometry over time at $p < 0.05$ significance level.

Cells expressing the lac repressor are smaller in size than those without

In order to investigate the effect of Lac repressor expression on cell size, the cell area was calculated from the cell segment length and a standard width for *E. coli* cells in pixels. In both the DnaE (figure 20) and DnaQ (figure 21) empty vector control strains, there was a significant increase in cell area compared to the first time point. For the DnaE strain, the initial mean cell area is 768.46±18.79 pixels and shows a significant increase by 50-70 minutes (878.1±31.3, p= 0.03 and 885.1±25.5, p=0.003). Similarly, the DnaQ strain has an initial mean area of 771.7±18.6 pixels, which increases to 860.7±21.4 pixels at 70-80 minutes (p= 0.009). Notably, The DnaE strain also demonstrates a significant increase at 0-10 minutes (884.3±24.1, p= 0.002).

There is either a decrease in cell area (DnaE) (figure 22) or no significant change in cell area (DnaQ) (figure 23) over the time course for the cells expressing the lac repressor. The DnaE lac repressor strain (figure 21) had an initial area of 740.4±10.1 pixels, which decreased significantly to 677.9±10.6 (p= 5.1e-05) by the end of the time course. A significant decrease in cell area can also be noted at the 10-20 (706.8±8.3, p= 0.04) and 60-70 (698.01±6.5, p= 0.002) minute time intervals. The mean cell area was greater for the empty vector controls in the case of both DnaE-mYPet and DnaQ-mYPet compared to the repressor-expressing strains. The mean cell areas for the controls were 828.8±6.8 pixels (DnaE) and 788.8±6.7 pixels (DnaQ) compared to the lower values of 716.4±2.6 (DnaE) and 645.6±3 (DnaQ) in strains expressing *LacI-mCherry*.

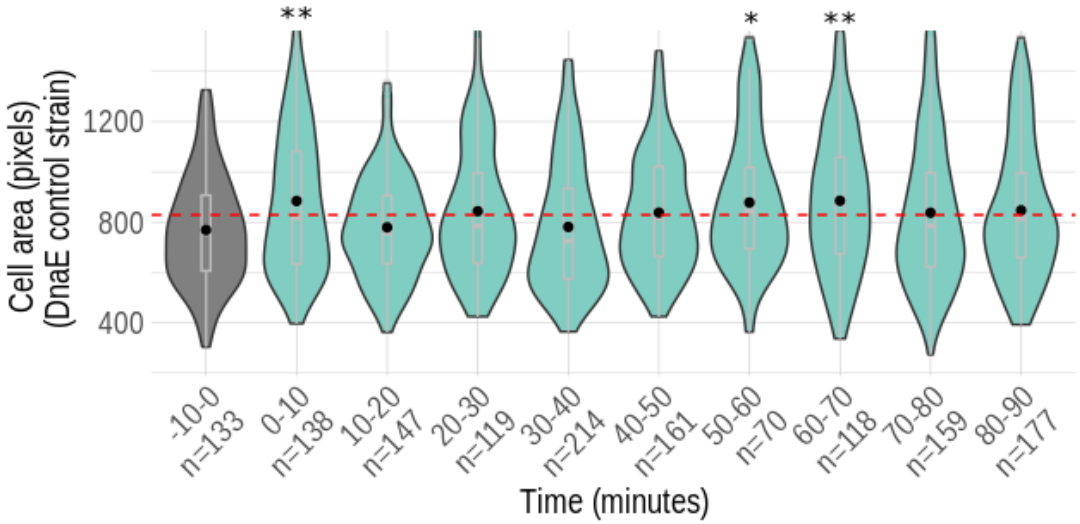

*Figure 20. Cell area in pixels of AS997 (DnaE-mYPet, empty vector). First time point represents the temperature downshift period. Red dotted line represents the mean cell area across all time points. Boxplots show median and interquartile range and black dots on graphs show means. (Mean and standard errors values: 768.5±18.8, 884.3±24.1, 779.1±16.4, 843.5±23.4, 7801±17.4, 837.9±18.3, 878.1±31.3, 885.1±25.5, 837.4±23.2, 847.01±20.3). Dunnett's tests were performed comparing all time points to the -10-0 minute interval, significant changes ($p < 0.05$) in cell area are as follows: 0-10 ($p = 0.002$), 50-60 ($p = 0.03$), 60-70 ($p = 0.003$). Stars show significant results ($p < 0.001$ '***', $p < 0.01$ '**', $p < 0.05$ '*').*

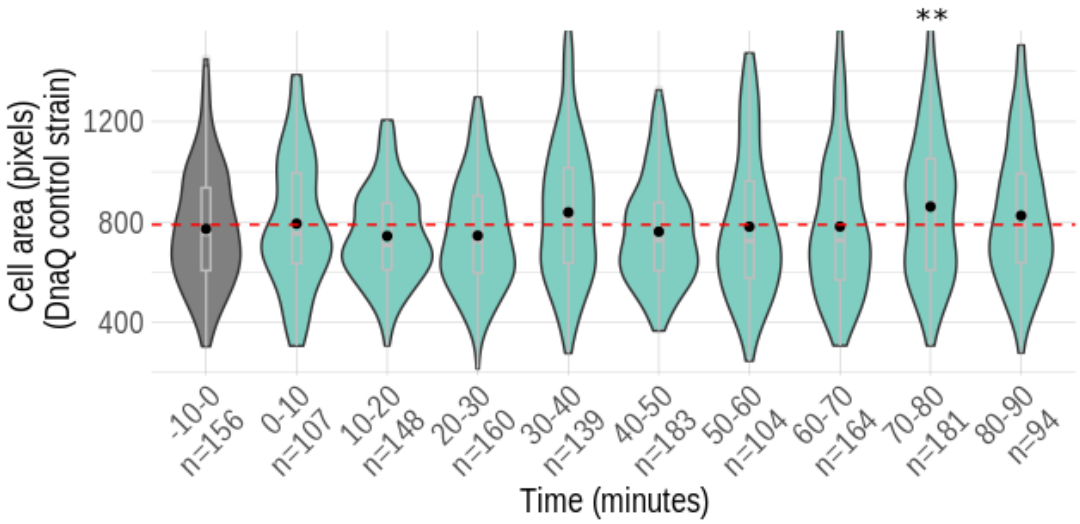

Figure 21. Cell area in pixels of AS993 (DnaQ-mYPet, empty vector). First time point represents the temperature downshift period. Red dotted line represents the mean cell area across all time points.

*Boxplots show median and interquartile range and black dots on graphs show means. (Mean and standard errors values: 771.7±18.6, 792.8±24.9, 743.2±15.3, 744.9±17.2, 837.8±23.4, 761±15.3, 780.9±27.9, 781.3±21.9, 860.7±21.4, 824.6±27.4). Dunnett's tests were performed comparing all time points to the -10-0 minute interval, significant changes ($p < 0.05$) in cell area are as follows: 70-80 ($p = 0.009$). Stars show significant results ($p < 0.001$ '***', $p < 0.01$ '**', $p < 0.05$ '*').*

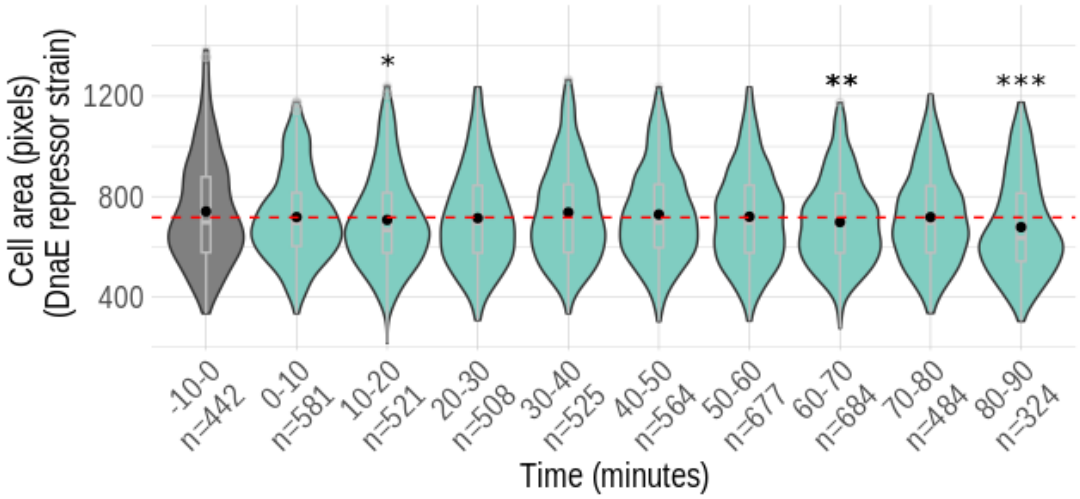

*Figure 22. Cell area in pixels of AS1000 (DnaE-mYPet, LacI-mCherry). First time point represents the temperature downshift period. Red dotted line represents the mean cell area across all time points. Boxplots show median and interquartile range and black dots on graphs show means. (Mean and standard errors values: 740.4±10.1, 717.8±7.3, 706.8±8.23, 713.8±8.6, 736.6±8.4, 728.3±7.8, 719.4±7.3, 698.01±6.5, 717.7±8.3, 677.9±10.6). Dunnett's tests were performed comparing all time points to the -10-0 minute interval, significant changes ($p < 0.05$) in cell area are as follows: 10-20 ($p = 0.04$), 60-70 ($p = 0.002$), 80-90 ($p = 5.1e-05$). Stars show significant results ($p < 0.001$ '***', $p < 0.01$ '**', $p < 0.05$ '*').*

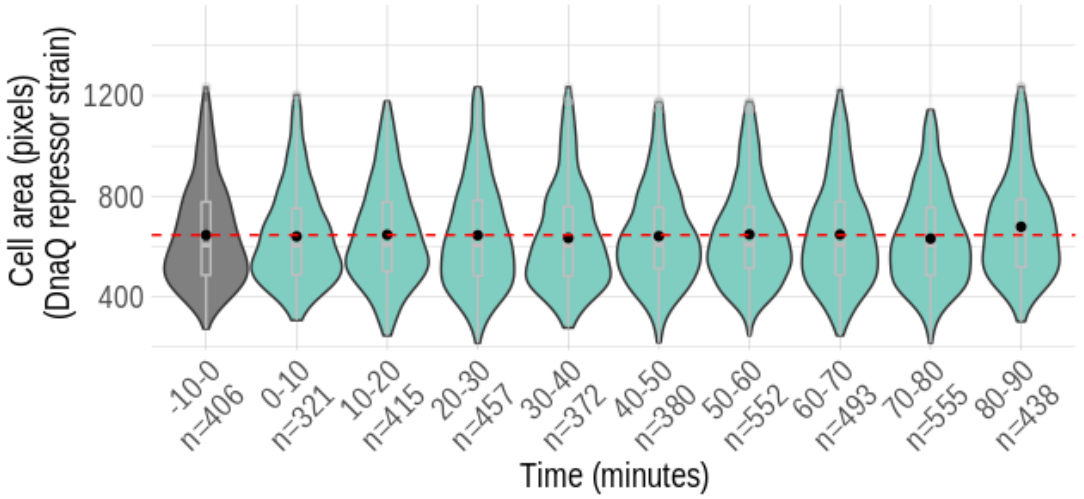

Figure 23. Cell area in pixels of AS996 (DnaQ-mYPet, LacI-mCherry). First time point represents the temperature downshift period. Red dotted line represents the mean cell area across all time points. Boxplots show median and interquartile range and black dots on graphs show means. (Mean and standard errors values: 645.3±9.9, 639.9±10.5, 646.4±9.8, 644.5±10.1, 633.5±10.5, 640.9±9.9, 648.01±8.2, 647.4±9.3, 631.2±8.01, 678.4±9.5). Dunnett's tests were performed comparing all time points to the -10-0 minute interval, with no significant changes found in cell area over time at $p < 0.05$ significance level.

DnaT foci and stoichiometry increase following replication initiation in cells expressing LacI-mCherry

To investigate the localisation of the replication restart protein DnaT in relation to the lac operator-repressor complexes, a fluorescent fusion of the protein labelled with mGFP was introduced into a strain containing the LacI-mCherry plasmid and a strain with the empty vector plasmid. These strains were imaged under the same conditions as the replisome components using dual-colour Slimfield microscopy to detect single molecules. However, it should be noted that due to inconsistencies in LacI-mCherry expression for this strain, this report focuses on single colour observations of DnaT. Therefore, the colocalisation between DnaT and binding of the lac repressor to the array has not been considered.

Single-molecule observations of the replication restart protein DnaT revealed a higher average stoichiometry across all time points combined (4.1±0.05) in the presence of the lac repressor (figure 24) compared to the stoichiometry of the empty vector (figure 25) control strain (3.3±0.05), which does not express the lac repressor. In addition, the empty vector strain saw a significant change in stoichiometry from the initial value of 3.5±0.1 at -10-0 minutes at only the 40-50 minute time point, with a decrease to 2.6±0.1 ($p= 8.2e-05$). Conversely, the *lac* repressor strain showed significant increases from 2.9±0.08 following the temperature downshift and consequent initiation of replication at all subsequent time points, reaching a maximum of 5.1±0.2 at 50-60 minutes ($p< 2e-16$).

In addition, the percentage of cells with DnaT foci is higher in the presence of the lac repressor. 38.9±0.01% of all cells (n = 5335) detected via imaging had detectable DnaT signal compared to 27.9±0.01% for the control strain (n = 2562). This difference is also prevalent in the single foci comparison, with values of 30.1±0.01% and 20.8±0.01% for the LacI-mCherry expressing and control strains, respectively. Fewer cells had two or more foci, with 8.7±0.004% of the repressor population found to have two or more foci and a slightly decreased percentage of 7.1±0.01% for the control population.

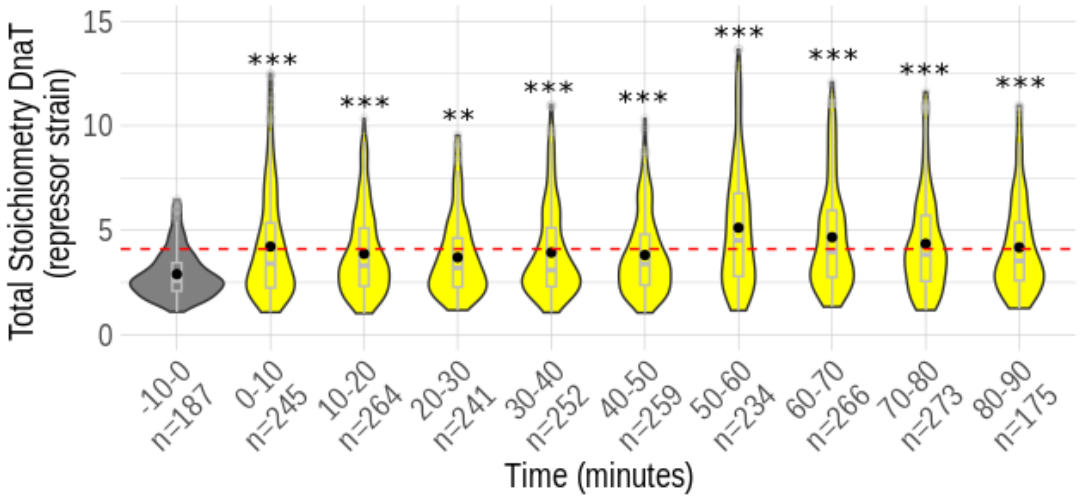

*Figure 24. DnaT total stoichiometry RH23 (*mGFP-dnaT*, lacI-mCherry). First time point represents the temperature downshift period. Red dotted line represents the mean stoichiometry across all time points. Boxplots show median and interquartile range and black dots on graphs show means. (Mean and standard errors values: 2.9±0.1, 4.2±0.2, 3.9±0.1, 3.7±0.1, 3.9±0.1, 3.8±0.1, 5.1±0.2, 4.7±0.2, 4.4±0.1, 4.2±0.2). Dunnett's tests were performed comparing all time points to the -10-0 minute interval, significant changes ($p < 0.05$) in stoichiometry are as follows: 0-10 ($p = 6.7e-09$), 10-20 ($p = 4.4e-05$), 20-30 ($p = 0.007$), 30-40 ($p = 1.3e-05$), 40-50 ($p = 0.0001$), 50-60 ($p < 2e-16$), 60-70 ($p = 4.4e-16$), 70-80 ($p = 3.3e-11$), 80-90 ($p = 8.2e-07$). Stars show significant results ($p < 0.001$ '***', $p < 0.01$ '**', $p < 0.05$ '*').*

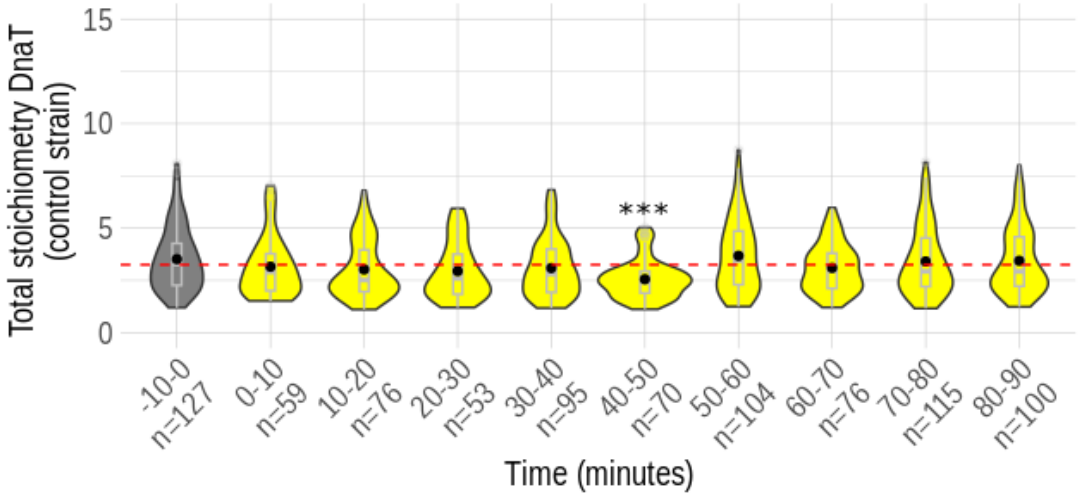

*Figure 25. DnaT total stoichiometry RH25 (*mGFP-dnaT*, empty vector). First time point represents the temperature downshift period. Red dotted line represents the mean stoichiometry across all time points. Boxplots show median and interquartile range and black dots on graphs show means. (Mean and standard errors values: 3.5±0.1, 3.2±0.2, 3.02±0.2, 2.9±0.2, 3.1±0.1, 2.6±0.1, 3.7±0.2, 3.1±0.1, 3.4±0.2, 3.4±0.2). Dunnett's tests were performed comparing all time points to the -10-0 minute interval, significant changes ($p < 0.05$) in stoichiometry are as follows: 40-50 ($p = 8.2e-05$). Stars show significant results ($p < 0.001$ '***', $p < 0.01$ '**', $p < 0.05$ '*').*

There is no difference in the growth rate of strains expressing the lac repressor compared to controls.

Growth rates for each strain included in this study were determined by diluting overnight culture grown in LB in minimal media. The LB media included IPTG to prevent the expression of the *lac* repressor before the change to minimal media and readings of OD_{600} over the time course (figure 26). The minimal media cultures were supplemented with arabinose and grown over a time period of 19 hours. This setup was designed to replicate the experimental conditions of both the slimfield microscopy and flow cytometry time course experiments.

There was variation in the doubling times of the strains, with RH28, the untagged repressor expressing strain, exhibiting a mean doubling time of 187.1±12.3 minutes. In contrast, the

strain with the DnaE fluorescently tagged repressor showed a mean doubling time of 297.01±10.9 minutes. These mean values represent the quickest and slowest rates for doubling time of the different cultures and reflect the variation in growth rates between strains in these experiments. However, further examination using statistical tests revealed no difference between strains despite this variation.

Pairwise comparisons were conducted using t-tests to statistically assess the differences between strains. These tests employed pooled standard deviations, and p-values were adjusted using the Bonferroni correction method to account for multiple comparisons. As a result of this statistical analysis, no significant differences were detected between any of the strains. This finding suggests that neither the presence of fluorescent tagging nor variations in lac repressor expression had a statistically significant effect on the growth rates of the strains at the $p < 0.05$ significance level.

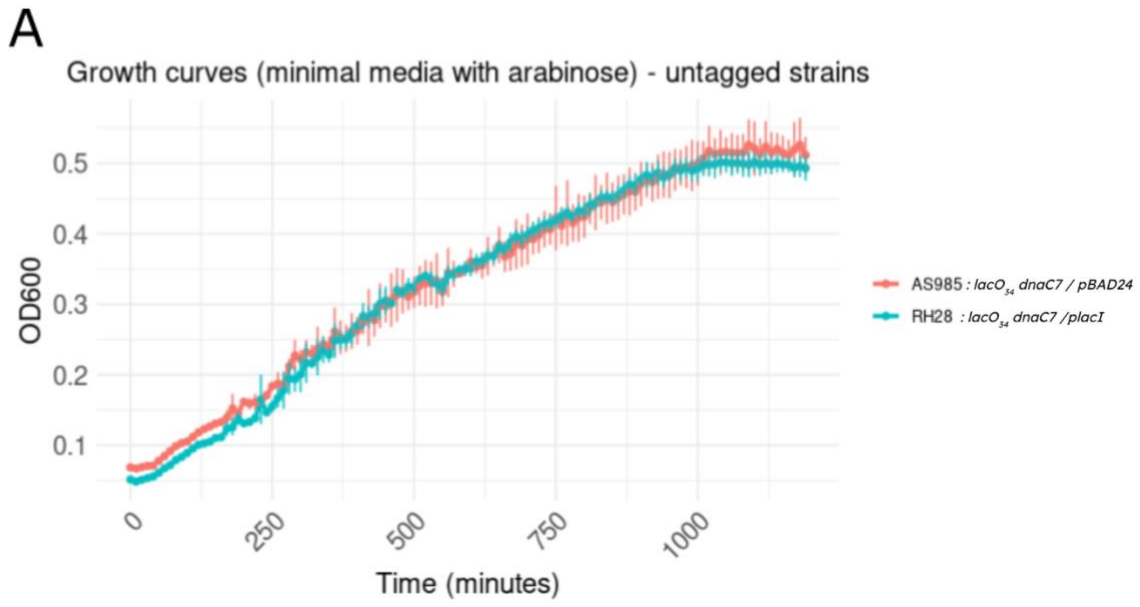

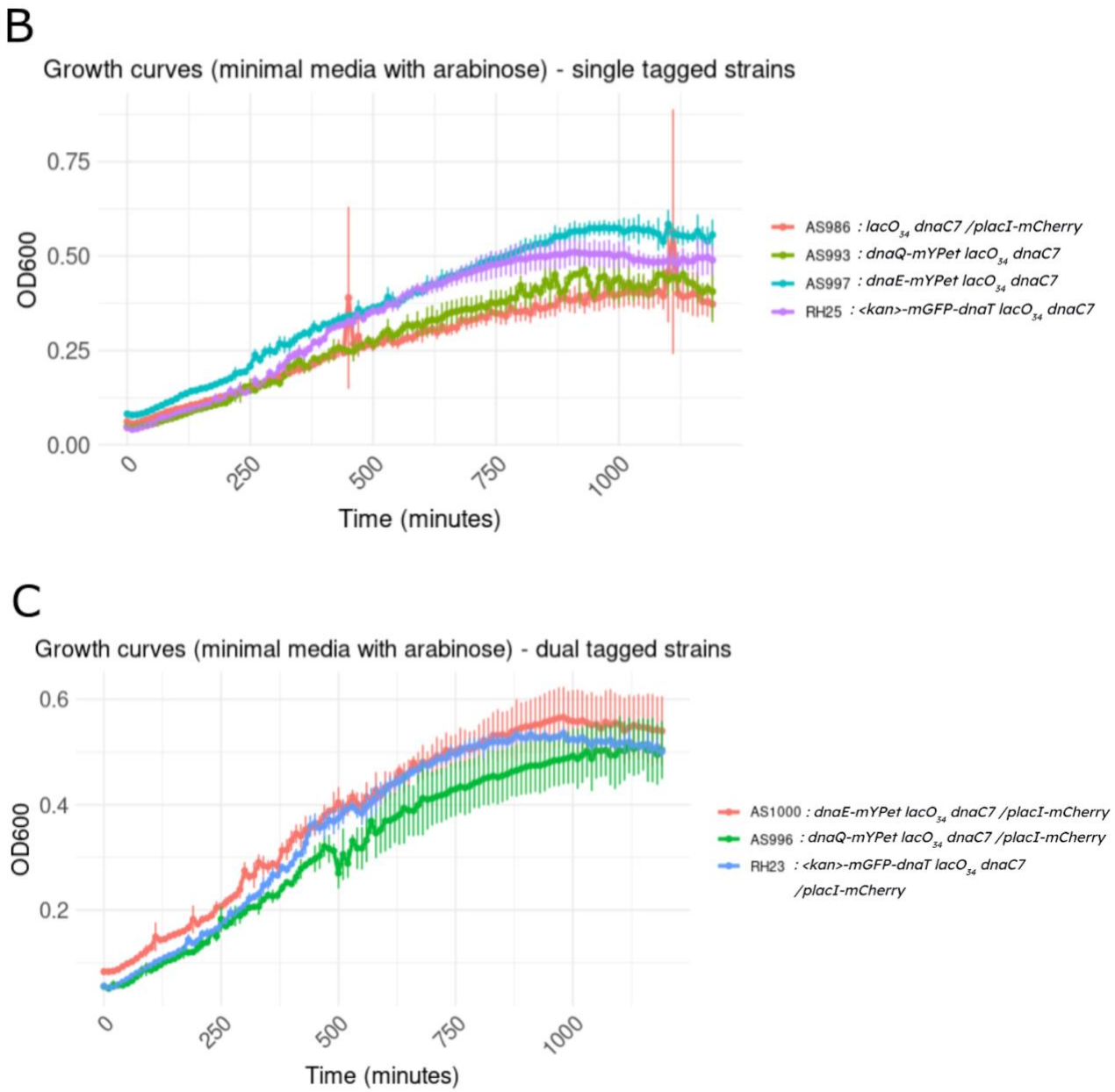

Figure 26. OD_{600} over the course of 19 hours (plotted in minutes) for all strains used in the study. Mean OD_{600} is plotted with the standard error at 10 minutes time intervals. A: Strains without fluorescent tagging B: Strains with single colour tagging C: Strains with dual colour tagging. (Doubling times for each strain are as follows in the order shown in the figure : AS1000: 297.01±10.9, AS985: 260.9±44.2, AS986: 242.6±6.1, AS993: 203.9±12.3, AS996: 231.1±16.4, AS997: 266.4±19.4, RH23: 187.7±34.6, RH25: 211.3±4.2, RH28: 187.1±19.4). Pairwise t-tests were conducted with pooled standard deviations to compare the doubling time of each strain to all other strains, p-values were adjusted using the Bonferroni method. No significant changes found in doubling time over time at $p < 0.05$ significance level.

Cells expressing the lac repressor have a higher proportion of incomplete chromosome copies compared to the control.

The number of chromosomes present in strains expressing the lac repressor compared to the empty vector strains was analysed using flow cytometry. Temperature-sensitive cultures were grown to the mid-log phase in minimal media at the permissive temperature and then incubated at 42℃ to synchronise the cultures. After 60 minutes, arabinose was added to the cultures to induce the lac repressor, and they were incubated for a further 30 minutes at 42℃. Cultures were then transferred to the 30℃ incubator to allow replication initiation, and samples were taken at ten minute intervals and treated with cephalexin to prevent cell division. Samples were incubated at 42℃ for a further 90 minutes and treated with ethanol.

DNA content (chromosome number) was tracked as a function of time (figure 27), with the progress of replication determined by the increase in DNA content from one chromosome to two chromosomes. A minimum of 50,000 events were recorded for each sample, with events comprising recordings of scattered light flowing through a laser. SYTOX Green binds to the nucleic acids and is excited by the laser. The resulting fluorescence measurement is a proxy for the DNA content of the cells.

Gates were created for peaks corresponding to one chromosome copy, two chromosome copies and the intermediate value between these peaks, representing incomplete chromosome replication. Across the majority of time points, no significant differences were found between the mean number of two copies detected as a percentage of all SYTOX events. The exceptions occurred at the 20 ($p=0.01$) and 40 ($p=0.045$) minute time points, with a slightly increased mean for the strain expressing the lac repressor (17.2 ± 0.4 and 20.03 ± 0.2) compared to the control (14.4 ± 0.2 and 18.7 ± 0.4).

Conversely, the repressor strain shows a significantly lower proportion of cells containing a single copy of the chromosome from 60 minutes onwards ($p= 0.03$). Most notably, there are striking differences in the proportion of intermediate values between the two peaks. With the exception of a non-significant difference between strains at 50 minutes, from 40 minutes until

the end of the time period, the repressor strain has a significantly higher proportion of intermediate events. By the 100 minute time point (p= 0.01), the repressor strain increased to a mean of 10.4±0.3 compared to the control strain with a mean of 8.1±0.1.

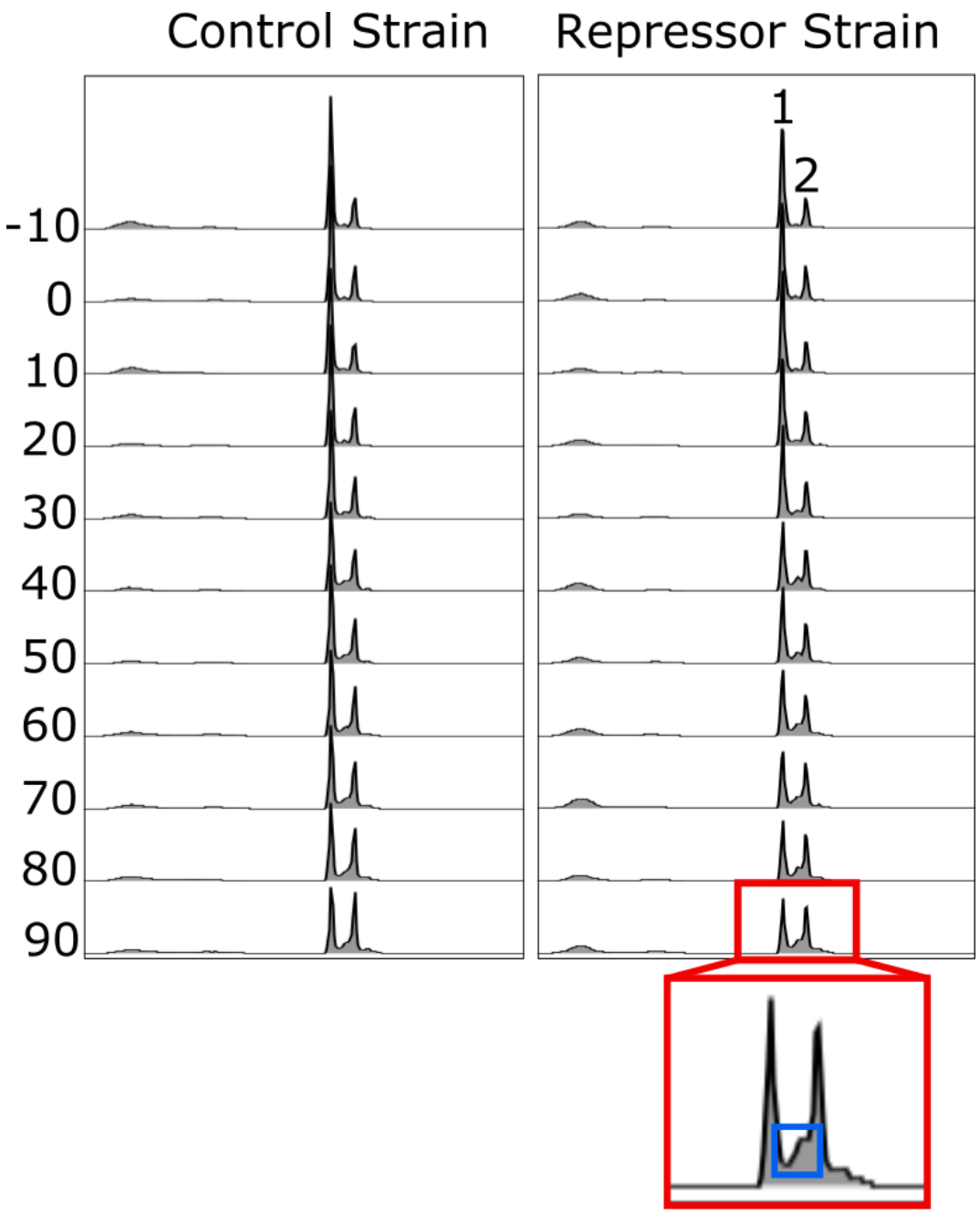

Figure 27. Flow cytometry plots for AS985 - empty vector control (left) and RH28 - repressor strain (right). First peak corresponds to one chromosome, second peak corresponds to two chromosomes. Samples taken over 100 minute time period - top graph at t = -10 minutes, bottom graph at t = 100 minutes. Blue box on zoom in indicates intermediate region between one and two chromosome copies.

Discussion

This study has explored the effects of the $LacO_{34}$ array as a proxy for stalled RNAP, which is known to be a frequent source of replication-transcription conflicts in *E. coli.* Single-molecule Slimfield imaging was used to determine the stoichiometry and localisation of both the lac repressor and the replisome. The results provide novel insights, pointing to a 'traffic jam' like model whereby consecutive rounds of replication initiation lead to the stacking up of replisomes, evidenced by an increase in stoichiometry at sites of the $LacO_{34}$ array. If the replisome cannot initially overcome the array, then it may dissociate and require replication restart, which could explain the subsequent decrease in stoichiometry. However, it is important to note that this thesis aims to set a baseline to explore replication block under further genetic perturbations such as deletions of restart proteins. As such, a key finding of this project relates to inefficacy of the array to block replication, resulting from low levels of operator occupancy as well as a low estimated value of LacI-mCherry copy number.

Lac repressor structure and function as a block to the replisome

The results of this study demonstrated that 21% of cells form lac repressor-operator complexes with stoichiometries ranging from 1.1 to 23.8 and with an average total stoichiometry approximating to four. The stoichiometry graphs show a periodicity of approximately four which is consistent with the established structure of the lac repressor (LacI) as tetrameric (Becker et al., 2024). The LacI tetramer is composed of two dimers, with one dimer binding the major lac operator, and consequently preventing transcription of the lac operon by RNA polymerase, and the second dimer binding one of the remaining auxiliary operators (Rutkauskas et al., 2009). The simultaneous binding of the dimers to two lac operator sites creates a loop around the DNA, which inhibits transcription. The observed range of stoichiometries up to a value of 24 suggests that there is evidence of higher-order complex formation in a proportion of the cells in which LacI is induced, corresponding to six LacI tetramers or 12 Lac operators.. In this study, 34 lac operators are present, indicating that a maximal occupation is not reached in most cases, with the majority of cells with LacI signal having only one LacI tetramer, potentially creating a less serious obstacle to the progression

of the replisome, that can be overcome via mRNA takeover (Brüning and Marians, 2021). Therefore, the high proportion of single repressors may explain the low replisome colocalization level in most cells, with the stoichiometry of linked LacI molecules being increased compared to the unlinked population.

In addition to the low stoichiometry of LacI, the majority (79%) of cells did not exhibit a detectable LacI-mCherry signal. This suggests that a significant proportion of cells have either an absence of complexes or that their presence is undetected by Slimfield microscopy. Given that the 34 operator sites present in the strains studied allow for the potential binding of multiple tetramers, it is possible that LacI is being removed or degraded by cellular mechanisms to facilitate the replisome's progression. For example, DNA helicases such as Rep and UvrD have been shown to assist in the removal of roadblocks ahead of the replication fork (Wollman et al., 2024). If this action of such helicases or other mechanisms of removal is responsible for the low detection of LacI, this suggests the $LacO_{34}$ array does not significantly affect the progression of replication in strains with repair and recombination machinery equivalent to that of wild-type. In addition, according to single-molecule studies by Elf et at., (2007), lac repressors diffuse along DNA and exhibit non-specific binding for approximately 90% of the time when searching for the operator, with the residence time found to be less than five milliseconds. Low rates of specific binding, coupled with high rates of transient non-specific binding may also explain the low level of detection. Therefore, dynamic binding and unbinding of LacI along the operator complex may lead to different tetramer complexes present at different stages of the imaging time period. However, it is also essential to note that the estimated copy numbers of LacI-mCherry, ranging from approximately 40 to 80 molecules per cell, point to the construct used in these experiments not efficiently expressing the repressor. Therefore, these results should be considered in the context of a lower level of repressor-operator binding than expected. However, it is possible that the low expression level could be the result of “dark’ molecules not visible due to delays in maturation times (Balleza, Kim and Cluzel, 2017; Hebisch et al., 2013). The maturation time of mCherry has been found to vary between *E. coli* strains. Shaner et al. (2004) estimated a maturation time of 15 minutes for mCherry expressed in *E. coli*. However, Hebisch et al. (2013) observed values randing from 45 to 114 minutes. Therefore, it is essential for future work the quantify the both the maturation times and expression levels of mCherry in the strains used for single-

molecule imaging experiments. In addition, recent data from the Leake lab has revealed a 50% reduction in copy number of the same molecule tagged with mCherry compared to YPet (personal communication – Aisha Syeda, University of York, unpublished data). The variation between copy numbers of different repliates coupled with the unexpected low expression level necessitates further investigation as a follow up to this project.

Furthermore, the results of the imaging experiments revealed temporal changes in the mean stoichiometry of the lac repressor throughout the cell cycle. The DnaE-mYPet strain shows an initial stoichiometry of approximately 2.9, which increases to 4.19 at 20-30 minutes. This time period may correspond to the duplication of the $LacO_{34}$ array, which is located at the argEC locus (4152.4 kb). This corresponds to an approximate time of 10 minutes for the replisomes to reach the region of the array in normal growth conditions, which may be delayed in the minimal media and low-temperature conditions. Similarly, by the 80-90 minute time point, the stoichiometry in both strains decreases to approximately 2.8 and 4.36 for DnaE and DnaQ strains, respectively. This reduction may indicate the impact of cell division, with each daughter cell inheriting a single copy of the $LacO_{34}$ array, leading to a corresponding drop in lac repressor occupancy. However, other results in this study demonstrated a slow doubling time and absence of cell division based on changes in cell area. SImilarly, the linked LacI population does not exhibit any significant changes in stoichiometry across the time course. As a result, it could be expected that this change arises as a result of different factors. Therefore, this change may be better explained by the transient non-specific interactions of the lac repressor with DNA away from the operator sites.

On the other hand, the stability of the mean lac repressor stoichiometry at sites of replisome stalling is supported by a recent study into the robustness of DNA looping generated by the lac system to perturbations within the cell. According to Chang et al. (2022), the presence of DNA loops allows for tight repression even in the event of multiple cell divisions. The study proposed that the efficacy of the repressor following cell division could result from multiple rebinding events and that this is a feature of DNA looping. This starkly contrasts observations in the absence of DNA loops, for which factors such as cell division and repressor concentration rendered gene regulation highly sensitive.

Replisome dynamics at the site of the conflict

The fluorescence microscopy data indicate that DnaE-mYPet is present in 59.8% of cells, with the majority of these cells (37.4%) displaying a single focus and a smaller proportion showing multiple foci. This distribution corresponds to previous studies which have identified similar foci distributions and overall detection by single-molecule imaging (Reyes-Lamothe et al., 2008). Interestingly, upon induction of the lac repressor, the percentage of cells with a single DnaE of DnaQ foci remains relatively stable, with the overall reduction in foci seeming to be brought about by a decrease in cells with two or more foci.

The occurrence of two distinct foci likely represent the two replication forks as sister replisomes travel bidirectionally around the chromosome. The model of DNA replication by the sister replisomes is a matter of debate, with different studies pointing to “train-track” whereby replisomes move independently of each other around opposite arms of the chromosome, or “factory” models whereby a single localisation of the replisomes remains stationary throughout replication, with DNA pulled into the complex. Recent studies have supported the former or a combination of both (Japaridze et al., 2020; Chen et al., 2023).

The presence of multiple foci in this study points to the separation of the replisomes following replication initiation and therefore, a mechanism with at least some elements of the train-track model, i.e. there is not a single replication factory for the entirety of the DNA replication process. However, it is notable that the majority of cells with replisome signal have only a single focus. This may point to a mechanism of factory-and-splitting model in which the initial physical association between sister replisomes establishes the efficiency of the replication process during a period of interdependence before “splitting” and carrying out genome duplication independently of each other, as presented by Chen et al. (2023).

Furthermore, the drop in frequency of cells with two foci, while the percentage with a single focus is maintained, following expression of LacI-mCherry may support the independence of replisomes after the locus presented in this study, with only one of the two replisomes affected rather than loss of both foci. The $LacO_{34}$ array is located at approximately 0.45 mb, which falls just below the threshold (0.6 Mb from the origin) for independent sister replisome

progression proposed by the 2023 study. Alternatively, it should be considered that frequent disengagement of the Pol III subassembly during DNA replication (Beattie et al., 2017) may result in cells having a single focus or multiple foci throughout the imaging period that does not necessarily correlate with the stage of DNA replication or the localisation within the cell.

Following on from the evidence of replisome disassembly throughout the replication cycle, the results of this study bring forward questions regarding the nature of Pol III disassembly in the event of obstacles to progression. There was a notable delay in peak stoichiometry for DnaQ compared to DnaE, and the resultant drop thereafter. If these changes are a result of stacking up of the replisomes at the site of the conflict, which is corrected by dissociation and replication restart, the time difference suggests that the core replisome disassembles progressively, with the epsilon subunit, responsible for proofreading, persisting for longer than the alpha subunit, which is responsible for the polymerase activity.

Numerous studies outline the role of DnaB as an anchor of the replisome, which persists for the entirety of the replication cycle despite the frequent exchange of other replisome components (Monachino et al., 2020; Spinks et al., 2021). However, there is little evidence to support or explain this difference in core replisome subunits. Beattie et al. (2017) observed subtle differences in the bound times at the replication fork of the alpha (DnaE) and epsilon (DnaQ) subunits using fluorescence recovery after photobleaching (FRAP), with the bound time of the epsilon subunit found to be greater, although without overlapping error bars. Even though this may require further study, the difference between replisome components indicates that the replisome is not simply stalling and then dislodging the block but must undergo disassembly to restart the replication process.

The time-course analysis showed a notable increase in the mean stoichiometry of both DnaE and DnaQ immediately following the downshift in temperature from 42℃ to 30℃. The unlinked stoichiometry values for DnaE (6.8 ± 0.3) and DnaQ (5.3 ± 0.2) rise to 7.8 ± 0.2 and 56 ± 0.3, respectively, during the 0-10 minutes period, and remain stable for the remaining time-course. This initial increase is indicative of enhanced replisome assembly consistent with the initiation of replication at the permissive temperature due to the action of the temperature-sensitive mutant *dnaC7*, which blocks replication elongation (Wechsler, 1975).

Single-molecule observations of the replisome components in the presence or absence of the lac repressor have revealed consistent mean total stoichiometries of DnaE and DnaQ when no LacI-mCherry is not expressed, with a notable reduction in total stoichiometry when the lac repressor is expressed. The observation that the presence of LacI-mCherry significantly reduces the overall stoichiometry of replisome components indicates that LacI-mCherry expression has broader impacts on DNA replication that are not localised to the site of the conflict. As a result of re-initiation of replication before the completion of previous rounds, cells may have multiple overlapping generations of replisomes (Dewachter et al., 2018), which is less prominent in bacteria growing in minimal media due to less rapid rates of cell division.

The cultures in this study may demonstrate lower stoichiometries in the presence of the lac repressor both as a result of the loss of replisomes as they dissociate from the replication fork (Pomerantz and O'Donnell, 2008) at the site of the array as well as due to a reduction in replication initiation. For example, the next generations of replisomes may not be initiated at the origin in the event of the highly conserved stringent response, which may be activated in the event of replication-transcription conflicts and result in inhibition of replication initiation (Mirkin and Mirkin, 2007). Furthermore, although this study is able to establish the low proportion of cells in the LacI-mCherry expressing state, it is important to note that the overall reduction in cells with signal is almost two-fold. Therefore, the cells categorised as experiencing more persistent blocks (those that are colocalised) may not be those faced with the most severe conflicts. Instead, the population exposed to the more serious blocks could be found in the subset with no replisome foci, potentially indicating replication fork collapse (Goehring et al., 2023).

In contrast, the linked stoichiometry results presented by this study present an insight into the interaction of the replisome with lac repressor-operator complexes. The observation that only a small proportion of cells experience sustained stalling of the replisome, which equates to the replisome component being localised to the lac repressor in approximately three percent of cells, demonstrates the well-developed mechanisms to overcome replication conflicts in *E. coli.* The data for DnaE and DnaQ shows a gradual increase over the time course,

reaching peaks of 12.7 ± 1.8 and 10.2 ± 1.2, respectively, between 50-70 minutes. This may correspond to an average value of four and three trimers, respectively.

This increase could reflect the 'traffic jam' like stacking up of replisomes at the site of the block, with consecutive replication forks impeded by the same block. This time point may represent the slow progression of the replication fork, with the 50 minutes being the time for the second fork to reach the block. Alternatively, although the dips in stoichiometry at earlier time points were found to be statistically insignificant, they may constitute the first replisome meeting the block and stalling before rescue with the restart proteins. Indeed, this observation warrants further investigation given the consistency between both DnaE and DnaQ, albeit at different time intervals prior to the significant peak.

The low percentage of cells exhibiting replisome stalling suggests that the $LacO_{34}$ construct does not significantly affect the replication cycle of wild-type cells. This conclusion is supported by spot tests conducted on *E. coli* with wild-type equivalent repair and recombination systems and those with mutations to inactivate or disrupt the function of the replication restart proteins (PriA, PriB, PriC) (personal communication - Christian Rudolph, Brunel University London, unpublished data). The growth of the wild-type strain containing the construct showed little difference in the presence and absence of the lac repressor. This indicates that inducing LacI-mCherry has little effect on the viability of the strain compared to the absence of expression.

Similarly, the results of growth tests on the repressor expressing and control strains showed no significant differences, indicating that the overall growth and viability of the cultures expressing LacI-mCherry are unaffected. Therefore, although the results of this study have identified replisomes at the site of the array, the majority of replisomes either seem to translocate across the array without being hindered by the complexes or are unaffected by the array due to cellular mechanisms to remove obstacles to the replication forks. This calls into question the fate of DNA replication in the case of a total loss of replisome signal, as is observed through the increased frequency of cells with no foci when exposed to LacI-mCherry expression. Although this represents a relatively large proportion of the population, it seems that the overall viability of the culture is not significantly affected. Again, this may be

explained by the dynamic nature of replisome exchange throughout the replication process, which is increased under replicative stress.

Reduced cell size in repressor cultures

The notable reduction in the cell area of cultures expressing LacI-mCherry indicates compromised cell metabolism presumably due to reduced rate or incomplete replication of the DNA due to impediments to the replication fork. However, the growth curves carried out in minimal media, and the presence of arabinose indicated no significant differences in the doubling time between repressor and control strains. Notably, the growth curves were carried out over a more extended time period (>18 hours) compared to the 100 minutes during which cells were imaged. This could represent a time in which cells respond to the block, which, in suboptimal minimal media growth conditions and 30℃ temperature, may lead to more pronounced differences in cell size compared to the control over a short period of time. Crucially, the growth curves did not take into account the synchronisation of cells. As a result, they do not show the initial recovery and replication initiation period following the downshift from 42℃. This contrasts the microscopy and flow cytometry experiments in which the LacI-mCherry is induced and time allowed for repressor-operator complex formation prior to replication initiation resulting from temperature downshift. Therefore, a repeat of the growth experiments could investigate the growth rate following synchronisation and incubation with arabinose rather than immediately after the induction of the lac repressor.

Changes in chromosome number

The results of the flow cytometry experiment demonstrate a gradual shift from the vast majority of cells having a single copy of the chromosome to an increased proportion with two copies and a decreased proportion with only one copy. This change over the time course is in agreement with cell cycle profiles achieved in previous flow cytometry experiments. Hawkins et al. (2022) found a gradual shift, as discussed, following the synchronisation of *E. coli* cultures and treatment with SYTOX Green. However, it is notable that their results showed a much more prominent shift between the peak at one and two copies. Furthermore, this study found that a smaller yet significant proportion of cells have already initiated replication before the downshift to the permissive temperature. In contrast to the protocol used in this project,

Hawkins et al. (2022) synchronised cells via incubation for two hours rather than 90 minutes and used a dnaA temperature-sensitive mutation as opposed to *dnaC7*, suggesting a potentially reduced efficacy of the synchronisation of the culture using the *dnaC7* mutation.

Nevertheless, the relatively small differences in flow cytometry profiles between the control and repressor strains point to similar rates of replication fork progression and indicate that the array does not effectively stall replisomes when looking at the culture as a whole. Despite this, the significant differences in the proportion of cells with an intermediate chromosome number (those falling between the peaks for one and two chromosomes) arise at approximately 50 minutes. This corresponds to the time point at which DnaE exhibits an increased stoichiometry colocalised to the $LacO_{34}$ array. It could, therefore, be concluded that this time point represents the point in the synchronised population at which a second replisome meets the previously stalled replisome, resulting in a build-up of replication machinery at the $LacO_{34}$ array.

DnaT stoichiometry and foci

An increase in cells with one or more DnaT foci was observed under the expression of the lac repressor, supporting the role of DnaT in the event of replication conflict and stalling. Previous studies have determined the role of DnaT as an essential replication protein, with mutants demonstrating similar phenotypic and stress responses to strains with PriA mutations (McCool et al., 2004). Although DnaT has been proposed to play a role in the recruitment of the DnaB helicase during restart (Lopper et al., 2007), there is little understanding of its fundamental function. In order to better understand the function of DnaT, this study quantified the stoichiometry across the 100 minute time course. The initial stoichiometry in both the repressor and empty vector strains approximated to a trimeric state. Previous studies have identified DnaT as both a homotrimer and a monomer-trimer equilibrium system ((Szymanski et al., 2013). However, early work by Arai et al. (1981) revealed biochemical data indicating the presence of DnaT oligomers up to the pentameric state.

Interestingly, the repressor strain demonstrates a peak stoichiometry of five at 50-60 minutes. Chen et al. (2019) proposed a “boomerang” mechanism of DnaT oligomerisation and

disassembly when interacting with ssDNA during replication restart. This model suggests that the presence of ssDNA promotes conformational changes in the C-terminal domain of DnaT that, in turn, promote oligomerisation from dimers into higher-order structures, including pentamers. The dissociation of ssDNA leads to the disassembly of the oligomer and reformation of DnaT dimers. The presence of DnaT predominantly as a dimer presented in the paper contradicts the results presented in this thesis. However, the concept of oligomerisation as part of the mechanism for DnaT-mediated replication restart, coupled with current literature pointing to the trimeric or monomer-timer equilibrium states is supported by the emergence of higher-order structures in the repressor strain.

Limitations

The synchronisation of cultures is essential to exploring the effects of LacI-mCherry expression complex on the progression of the replisome. This is mediated by the introduction of the Dnac7 temperature-sensitive mutation. DnaC forms a complex with the DnaB helicase in order for DnaB to bind at the origin of replication. However, the dislocation of DnaC is necessary to allow DnaB to unwind the DNA duplex. Therefore, DnaC is considered a checkpoint which marks the change from replication initiation, following the loading of DnaB at oriC, to replication elongation.

Despite the introduction of DnaC7 for all strains used in this study, results from the flow cytometry experiments indicate that a smaller but notable proportion of the population contains two chromosome copies even at the zero-minute time point. Consequently, it seems that even following incubation for a prolonged time period at the non-permissive temperature, some cells are experiencing replication initiation either due to the mutation not being sufficient to prevent replication initiation in all cases or due to the short period of time during which cells are at room temperature during the step of aliquoting 100ul and treatment with cephalexin.

Similarly, the temperature sensitive nature of the experiments made them difficult to replicate precisely. For example, the microscopy experiment was adapted from an initial protocol so that arabinose was added to the slide overlay, and incubation was carried out in

a temperature-controlled chamber to mitigate time lost when locating cells and focusing the microscope. However, this meant that up to four minutes elapsed between the initial induction of LacI-mCherry and incubation at the non-permissive temperature. As a result, it is possible for replication to have been initiated in a proportion of the population. Since the DnaC7 does not prevent the continuation of DNA replication following initiation, this may lead to a number of replisomes meeting or passing the $LacO_{34}$ array before the time period of imaging.

One possible solution would be to carry out microscopy experiments using a microfluidic device to allow for incubation at a non-permissive temperature and the introduction of arabinose into the growth media during the incubation. In addition, further investigation into the acclimation of the culture to changes in temperature would increase the robustness of the study. The protocol used accounted for approximately ten minutes for the microscope chamber to decrease from 42℃ to 30℃. However, this could be investigated further to determine the time required for replication to initiate in the majority of cells. This also applies to the flow cytometry experiments, in which there seems to be lower rates of replication initiation. Repeats and further optimisation of the experiment are necessary to validate the results and ensure consistency with the imaging experimental protocol.

This uncertainty produced a level of variability in the stages of replication of the cells being imaged, which, although mitigated to an extent by the large sample size, may affect the time periods at which changes in replisome stoichiometry are observed. However, it would be difficult to eliminate all variability in replication initiation even with these recommendations, with the potential for some cells to initiate before reaching the permissive temperature, whilst others may require more prolonged incubation at 30℃ to allow for the proper function of DnaC7. Finally, as discussed, it is essential to accurately quantify the expression levels of LacI-mCherry as well as the maturation time of the fluorescent protein. It is possible that increased incubation times at 42℃ prior to imaging could aid in both the synchronisation of the culture as well as increased expression of LacI-mCherry and maturation of the fluorescent protein.

Future perspectives

Aside from potential future directions to account for the limitations of this study, there are a number of potential pathways for future work arising from these results to continue to elucidate the mechanism of replication-transcription conflicts. Firstly, an important control to include in future work would be a strain containing the LacI-mCherry plasmid without the *lacO*$_{34}$ array. This would help to determine if it is the presence of LacI or the complex formed by binding to the operator site that leads to the observed changes in replisome stoichiometry and cell morphology presented here. Given that, only a small proportion of the population is affected by the expression of LacI-mCherry and the replication restart proteins likely play a significant role in rescuing stalled fork, an interesting approach would be to study the effects of inactivating the genes encoding these proteins. This would support the hypothesis of replisome dissociation and restart.

The evidence for reduced viability of strains containing Pri mutants would suggest that the number of cells with detected colocalisation between the replisome and the array may increase. Alternatively, it may lead to a reduction in cells with replisome signal as the machinery dissociates and cannot be restarted. Furthermore, by examining a range of proteins involved in replication and repair it could be possible to create a more detailed model of the conflict resolution, such as by investigating proteins involved following fork collapse. Similarly, the low percentage of cells with Lac repressor signal could be explored by introducing mutants of replicative helicases. If the low detection is due to the removal of the repressor rather than transient or low levels of successful binding, these mutant strains should result in an increased LacI-mCherry signal.

Notably, there were subtle differences in the changes in stoichiometry of DnaE compared to DnaQ over the time course. This may point to a stepwise dissociation of the replication machinery. Therefore, by repeating the single-molecule imaging experiments under the same conditions, different subunits of the replisome, including those that are not core replisome proteins, can be compared to DnaE and DnaQ as well as existing data on replication machinery dwell times and stoichiometry. In particular, it would be interesting to explore the dynamics of DnaB. DnaB is the helicase and has been identified by numerous studies (Monachino et al.,

2020; Spinks et al., 2021) as exhibiting a longer dwell time and, therefore, acting as a stable anchor to the replisome as it translocates across the DNA template. A delay in the reduction of DnaB stoichiometry compared to the core replisome could indicate the dissociation of the replisome and the dynamic exchange of replisome components followed by its eventual restart and progression. Alternatively, a concurrent drop in stoichiometry linked to the $LacO_{34}$ array between DnaB and other components may indicate a shorter period of replisome stalling, with the replication machinery able to overcome the block without additional cellular mechanisms, as may be the case in less severe conflicts.

Although the results of the imaging experiments presented in this study are generally in agreement with the tetrameric structure of the lac repressor, the ranges of occupancy of the operator array provoke further questioning about the formation of the complex and how variation in stoichiometry can be explained. The current literature presents a looping of LacI around the DNA, with one dimer bound to the major lac operator and the other bound to a second operator. This has been demonstrated as being a stable interaction, whilst the search for the operator site involves transient non-specific binding. Future studies could explore the maximal occupancy of different numbers of lac operator sites by looking at single-colour, single-molecule imaging or tagging the operator sites and quantifying the degree of colocalisation using dual-colour imaging. Conversely, an *in vitro* approach may be more useful to isolate the interaction between the operator sites and the repressor without the impact of *in vivo* processes that act to remove DNA-bound proteins.

Another exciting prospect for follow-up studies could be the focus on tracking the replisome and Lac repressor over the same time course in a single cell. This approach would involve challenges, such as the low proportion of cells with stalled replisomes and the impact of bleaching on the fluorescent signal, which would necessitate fewer frames to be imaged for each acquisition. However, it would determine the fate of the lac repressor upon impact from the replisome, with the potential for loss of repressor signal or indication of a stable complex. Furthermore, the period during which the replisome is stationary at the site of a block could be quantified. This approach could also confirm the role of replication restart proteins in overcoming blocks to replication, with the possibility that a reduction in replisome signal

would be followed by an accumulation of restart proteins colocalised to the repressor-operator complex.

Conclusions

The temporal change in the mean linked stoichiometry of replisome components suggests that the stalling of the replisome is followed by further collisions from new rounds of replication. Cell division at around the 70-minute time point could be a possible explanation for the observed drop in stoichiometry after the peak. However, the quantification of cell size points to a reduced area for cells across the entire time period rather than a gradual increase followed by a drop in area, which would be indicative of cell growth and division. In fact, the reduced cell area may instead point to a possible delay in cell division owing to a reduced rate or incomplete replication of the DNA. Therefore, the gradual increase for both DnaE and DnaQ, followed by a drop in stoichiometry may be attributed to either the dislodgement of the repressor-operator complex or dissociation of the replisome and replication restart (figure 28).

Given that the $LacO_{34}$ array is present on the leading strand, it could be expected that the displacement of the complex is necessary for fork progression (Brüning and Marians, 2021). Despite this, the stable stoichiometry of the total LacI signal and the increased yet stable stoichiometry across the time period of the LacI signal colocalised to the replisome would indicate that although few cells appear to form the repressor complex, the complexes that form successfully remain relatively stable. This may suggest that although there are likely to be other cellular processes involved, such as the activity of accessory replicative helicases removing obstacles to replication ahead of the replication fork, the impact of the replication machinery is not enough to dislodge the more severe replication blocks. However, it is important to note that the low colocalisation rate might reflect the replisome's efficiency in overcoming simple blocks. It is possible that the model of bypass presented by Brüning and Marians (2021), in which dislodgement of the block is a prerequisite, is the predominant mechanism of replication fork progression. This may also explain the low detection of LacI-

mCherry foci, with the block having a minimal impact on replisome progression and therefore demonstrating only a transient colocalisation as the repressor is dislodged and the replisome 'skips' the site of conflict. In addition, low rates of repressor-operator complex formation may arise from selection for the loss of the $LacO_{34}$ construct. Cells without the construct would likely have a growth advantage and could increase in frequency in the population.

Therefore, although this may be the primary contributing factor to the progression of the replisome, a number of results in this study suggest a different explanation for the observation of the "stacking" dynamics. The increased detection of foci and stoichiometry of the replication restart protein DnaT in cells expressing the lac repressor suggests that the block gives rise to increased replisome dissociation, requiring the activity of the restart proteins to maintain cell viability and that this activity increases with more persistent blocks as further replisomes stack up at the site of conflict. Furthermore, the stability of LacI stoichiometry colocalised to replisome components indicates that the repressor remains bound to the DNA template even as the replisomes stack up and eventually overcome the block. Finally, the delay in stoichiometry changes in DnaQ compared to DnaE point to a gradual dissociation of the replisome rather than direct translocation either across the DNA template or via mRNA takeover. Consequently, the potential translocation of the replisome across the site of the block, following dissociation from the DNA and replication restart, could be the most probable explanation.

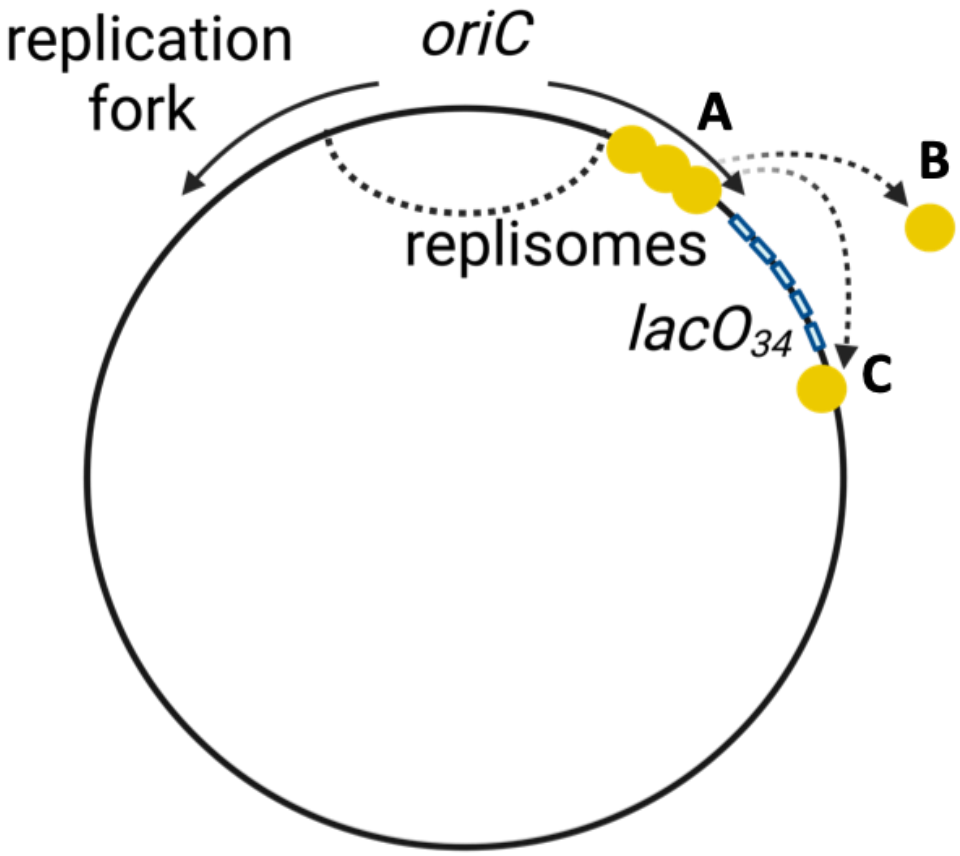

Figure 28. Dynamics of the replisome as it reaches the block: A: Replisome 'traffic jam': A: Multiple replisomes stack up as they are unable to translocate across the DNA template. Decreases in DnaE-mYPet stoichiometry could be attributed to B: Replisome dissociates: Immobile and therefore inactive replisomes may dissociate from the DNA. C: Replisome overcomes block: Replisomes may dislodge the block and can therefore continue to replicate the DNA template.

These results demonstrate that the block had little effect on the progression of the replisome across the population of cells that were imaged. However, a notable decrease in total replisome stoichiometry was observed when the lac repressor was present compared to the empty vector control, as well as a reduced size phenotype. Despite these effects, the overall impact on replication and cell viability across the population appears to be low, evidenced by a flow cytometry cell cycle profile similar to that of the control.

Although most cells are able to navigate across the block, the population that meets with more serious and persistent obstacles is unable to complete replication, with the potential for fork collapse in these cases, shown by an increase in intermediate flow cytometry peaks. The efficiency of cells in regulating the block can be explained by the presence of replication restart proteins, which are known to be essential in wild-type populations due to frequent replication fork stalling even in optimal growth conditions. It is possible that a higher proportion of cells experience replisome stalling at the block than is shown by the colocalised data, but the rapid action of restart proteins allows the quick and efficient continuation of the replisome at the locus. Therefore, the colocalisation may be brief and not detected at the population level, with no increase in stoichiometry since the previous replisome is no longer stalled.

Overall, this study provides strong evidence to support the importance of single-molecule studies when investigating fundamental questions in cell biology. Qualitative results of survival tests or even the quantitative metrics, such as doubling time provided by growth curves, do not accurately depict the impact of the $Lac0_{34}$. Complex as a block to replication. The results of such tests indicate that the block has no significant effect on cell viability. However, the imaging data in this study reveals changes at the single-molecule level that point to the congregation of multiple replisomes at sites of conflict. Furthermore, the differences in DnaT stoichiometry in cells exposed to the block give indications as to the role of replication restart in overcoming replication conflict, with the increase in cells with foci as can be determined with conventional fluorescence microscopy not conveying the complete picture of potential DnaT oligomerisation. This project sets up further investigation into the dynamics of replication block, and provides a basis for optimising the protocols of single-molcule imaging experiments to aid in accuracy of timing of the molecular events that occur. Future perspectives should focus on the role of the replication restart proteins and the potential changes in the severity of the block when the mechanism of restart is disrupted. This could involve tracking the replisome over the course of the cell cycle in single cells rather than looking at the overall population.

References

Adam J.M. Wollman, Syeda, A.H., Jamieson A.L. Howard, Payne-Dwyer, A., Leech, A., Dominika Warecka, Guy, C., McGlynn, P., Hawkins, M. and Leake, M.C. (2024). Tetrameric UvrD Helicase Is Located at the E. Coli Replisome due to Frequent Replication Blocks. *Journal of Molecular Biology*, [online] 436(2), pp.168369–168369. doi:https://doi.org/10.1016/j.jmb.2023.168369.

Aleksandre Japaridze, Christos Gogou, Jacob, Huyen My Nguyen and Dekker, C. (2020). Direct observation of independently moving replisomes in Escherichia coli. *Nature Communications*, [online] 11(1). doi:https://doi.org/10.1038/s41467-020-16946-7.

Antony, E. and Lohman, T.M. (2019). Dynamics of E. coli single stranded DNA binding (SSB) protein-DNA complexes. *Seminars in Cell & Developmental Biology*, [online] 86, pp.102–111. doi:https://doi.org/10.1016/j.semcdb.2018.03.017.

Arai, K., McMacken, R., Yasuda, S. and Kornberg, A. (1981). Purification and properties of Escherichia coli protein i, a prepriming protein in phi X174 DNA replication. *Journal of Biological Chemistry*, 256(10), pp.5281–5286. doi:https://doi.org/10.1016/s0021-9258(19)69399-3.

Balleza, E., Kim, J.M. and Cluzel, P. (2017). Systematic characterization of maturation time of fluorescent proteins in living cells. Nature Methods, 15(1), pp.47–51. doi:https://doi.org/10.1038/nmeth.4509.

Beattie, T.R., Kapadia, N., Nicolas, E., Uphoff, S., Wollman, A.J., Leake, M.C. and Reyes-Lamothe, R. (2017). Frequent exchange of the DNA polymerase during bacterial chromosome replication. *eLife*, [online] 6, p.e21763. doi:https://doi.org/10.7554/eLife.21763.

Beattie, T.R. and Reyes-Lamothe, R. (2015). A Replisomeâ€™s journey through the bacterial chromosome. *Frontiers in Microbiology*, 6. doi:https://doi.org/10.3389/fmicb.2015.00562.

Becker, N.A., Peters, J.P., Lewis, E., Daby, C., Clark, K. and Maher, L. (2024). Engineered transcription activator-like effector dimer proteins confer DNA loop-dependent gene

repression comparable to Lac repressor. *Nucleic Acids Research*. [online] doi:https://doi.org/10.1093/nar/gkae656.

Blattner, F.R. (1997). The Complete Genome Sequence of Escherichia coli K-12. *Science*, 277(5331), pp.1453–1462. doi:https://doi.org/10.1126/science.277.5331.1453.

Boubakri, H., de Septenville, A.L., Viguera, E. and Michel, B. (2010). The helicases DinG, Rep and UvrD cooperate to promote replication across transcription units in vivo. *The EMBO Journal*, 29(1), pp.278–278. doi:https://doi.org/10.1038/emboj.2009.390.

Brüning, J.-G. and Marians, K.J. (2021). Bypass of complex co-directional replication-transcription collisions by replisome skipping. *Nucleic Acids Research*, 49(17), pp.9870–9885. doi:https://doi.org/10.1093/nar/gkab760.

Burby, P.E. and Simmons, L.A. (2019). Regulation of Cell Division in Bacteria by Monitoring Genome Integrity and DNA Replication Status. *Journal of Bacteriology*, 202(2). doi:https://doi.org/10.1128/jb.00408-19.

Chang, C., Garcia-Alcala, M., Saiz, L., Jose and Philippe Cluzel (2022). Robustness of DNA looping across multiple cell divisions in individual bacteria. *Proceedings of the National Academy of Sciences*, 119(33). doi:https://doi.org/10.1073/pnas.2200061119.

Chen, K.-L., Huang, Y.-H., liao, J.-F., Lee, W.-C. and Huang, C.-Y. (2019). Crystal structure of the C-terminal domain of the primosomal DnaT protein: Insights into a new oligomerization mechanism. *Biochemical and Biophysical Research Communications*, 511(1), pp.1–6. doi:https://doi.org/10.1016/j.bbrc.2019.02.026.

Cox, M.M., Goodman, M.F., Kreuzer, K.N., Sherratt, D.J., Sandler, S.J. and Marians, K.J. (2000). The importance of repairing stalled replication forks. *Nature*, 404(6773), pp.37–41. doi:https://doi.org/10.1038/35003501.

Dewachter, L., Verstraeten, N., Fauvart, M. and Michiels, J. (2018). An integrative view of cell cycle control in Escherichia coli. *FEMS Microbiology Reviews*, [online] 42(2), pp.116–136. doi:https://doi.org/10.1093/femsre/fuy005.

Duckworth, A.T., Ducos, P.L., McMillan, S.D., Satyshur, K.A., Blumenthal, K.H., Deorio, H.R., Larson, J.A., Sandler, S.J., Grant, T. and Keck, J.L. (2023). Replication fork binding triggers structural changes in the PriA helicase that govern DNA replication restart in E. coli. *Nature Communications*, 14(1). doi:https://doi.org/10.1038/s41467-023-38144-x.

Eduardo and Danchin, A. (2003). Gene essentiality determines chromosome organisation in bacteria. *Nucleic Acids Research*, 31(22), pp.6570–6577. doi:https://doi.org/10.1093/nar/gkg859.

Elf, J., Li, G.-W. and Xie, X.S. (2007). Probing Transcription Factor Dynamics at the Single-Molecule Level in a Living Cell. *Science*, 316(5828), pp.1191–1194. doi:https://doi.org/10.1126/science.1141967.

Fujiyama, S., Abe, Y., Tani, J., Urabe, M., Sato, K., Aramaki, T., Katayama, T. and Ueda, T. (2014). Structure and mechanism of the primosome protein DnaT– functional structures for homotrimerization, dissociation of ssDNA from the PriB·ssDNA complex, and formation of the DnaT·ssDNA complex. *The FEBS journal*, 281(23), pp.5356–5370. doi:https://doi.org/10.1111/febs.13080.

Goehring, L., Huang, T.T. and Smith, D.J. (2023). Transcription–Replication Conflicts as a Source of Genome Instability. *Annual Review of Genetics*, 57(1). doi:https://doi.org/10.1146/annurev-genet-080320-031523.

Grieb, M.S., Nivina, A., Cheeseman, B.L., Hartmann, A., Mazel, D. and Schlierf, M. (2017). Dynamic stepwise opening of integron attC DNA hairpins by SSB prevents toxicity and ensures functionality. *Nucleic Acids Research*, 45(18), pp.10555–10563. doi:https://doi.org/10.1093/nar/gkx670.

Guy, C.P., Atkinson, J., Gupta, M.K., Mahdi, A.A., Gwynn, E.J., Rudolph, C.J., Moon, P.B., van Knippenberg, I.C., Cadman, C.J., Dillingham, M.S., Lloyd, R.G. and McGlynn, P. (2009). Rep Provides a Second Motor at the Replisome to Promote Duplication of Protein-Bound DNA. *Molecular Cell*, 36(4), pp.654–666. doi:https://doi.org/10.1016/j.molcel.2009.11.009.

Guy, L. and Roten, C.-A.H. (2004). Genometric analyses of the organization of circular chromosomes: a universal pressure determines the direction of ribosomal RNA genes

transcription relative to chromosome replication. *Gene*, 340(1), pp.45–52. doi:https://doi.org/10.1016/j.gene.2004.06.056.

Hamperl, S. and Cimprich, K.A. (2016). Conflict Resolution in the Genome: How Transcription and Replication Make It Work. *Cell*, [online] 167(6), pp.1455–1467. doi:https://doi.org/10.1016/j.cell.2016.09.053.

Hawkins, M., Atkinson, J. and McGlynn, P. (2022). Escherichia coli Chromosome Copy Number Measurement Using Flow Cytometry Analysis. *Methods in molecular biology*, pp.145–153. doi:https://doi.org/10.1007/978-1-0716-2221-6_11.

Hebisch, E., Knebel, J., Landsberg, J., Frey, E. and Leisner, M. (2013). High Variation of Fluorescence Protein Maturation Times in Closely Related Escherichia coli Strains. PLoS ONE, 8(10), p.e75991. doi:https://doi.org/10.1371/journal.pone.0075991.

Heller, R.C. and Marians, K.J. (2005). The Disposition of Nascent Strands at Stalled Replication Forks Dictates the Pathway of Replisome Loading during Restart. *Molecular Cell*, 17(5), pp.733–743. doi:https://doi.org/10.1016/j.molcel.2005.01.019.

Langston, L.D., Indiani, C. and O'Donnell, M. (2009). Whither the replisome: Emerging perspectives on the dynamic nature of the DNA replication machinery. *Cell Cycle*, 8(17), pp.2686–2691. doi:https://doi.org/10.4161/cc.8.17.9390.

Lestini, R. and MichelB. (2008). UvrD and UvrD252 Counteract RecQ, RecJ, and RecFOR in a rep Mutant of Escherichia coli. *Journal of Bacteriology*, 190(17), pp.5995–6001. doi:https://doi.org/10.1128/jb.00620-08.

Lin, Y.-L. and Pasero, P. (2017). Transcription-Replication Conflicts: Orientation Matters. *Cell*, [online] 170(4), pp.603–604. doi:https://doi.org/10.1016/j.cell.2017.07.040.

Lopper, M., Boonsombat, R., Sandler, S.J. and Keck, J.L. (2007). A Hand-Off Mechanism for Primosome Assembly in Replication Restart. *Molecular Cell*, 26(6), pp.781–793. doi:https://doi.org/10.1016/j.molcel.2007.05.012.

Mangiameli, S.M., Merrikh, C.N., Wiggins, P.A. and Merrikh, H. (2017). Transcription leads to pervasive replisome instability in bacteria. *eLife*, 6. doi:https://doi.org/10.7554/elife.19848.

Marceau, A.H. (2012). Functions of single-strand DNA-binding proteins in DNA replication, recombination, and repair. *Methods in Molecular Biology (Clifton, N.J.)*, [online] 922, pp.1–21. doi:https://doi.org/10.1007/978-1-62703-032-8_1.

Margulies, C. and Kaguni, J.M. (1996). Ordered and Sequential Binding of DnaA Protein to oriC, the Chromosomal Origin of Escherichia coli*. *Journal of Biological Chemistry*, [online] 271(29), pp.17035–17040. doi:https://doi.org/10.1074/jbc.271.29.17035.

McCool, J.D., Ford, C.M. and Sandler, S.J. (2004). A dnaT Mutant With Phenotypes Similar to Those of a priA2::kan Mutant in Escherichia coli K-12. *Genetics*, 167(2), pp.569–578. doi:https://doi.org/10.1534/genetics.103.025296.

McCool, J.D. and Sandler, S.J. (2001). Effects of mutations involving cell division, recombination, and chromosome dimer resolution on a priA2::kan mutant. *Proceedings of the National Academy of Sciences*, 98(15), pp.8203–8210. doi:https://doi.org/10.1073/pnas.121007698.

McHenry, C.S. (2011). DNA Replicases from a Bacterial Perspective. *Annual Review of Biochemistry*, 80(1), pp.403–436. doi:https://doi.org/10.1146/annurev-biochem-061208-091655.

Michel, B., Sinha, A.K. and David (2018). Replication Fork Breakage and Restart in Escherichia coli. *Microbiology and Molecular Biology Reviews*, 82(3). doi:https://doi.org/10.1128/mmbr.00013-18.

Miller, H., Zhou, Z., Wollman, A.J.M. and Leake, M.C. (2015). Superresolution imaging of single DNA molecules using stochastic photoblinking of minor groove and intercalating dyes. *Methods*, 88, pp.81–88. doi:https://doi.org/10.1016/j.ymeth.2015.01.010.

Mirkin, E.V. and Mirkin, S.M. (2005). Mechanisms of Transcription-Replication Collisions in Bacteria. *Molecular and Cellular Biology*, 25(3), pp.888–895. doi:https://doi.org/10.1128/mcb.25.3.888-895.2005.

Mirkin, E.V. and Mirkin, S.M. (2007). Replication Fork Stalling at Natural Impediments. *Microbiology and Molecular Biology Reviews*, 71(1), pp.13–35. doi:https://doi.org/10.1128/mmbr.00030-06.

Monachino, E., Jergic, S., Lewis, J.S., Xu, Z.-Q., Lo, A.T.Y., O'Shea, V.L., Berger, J.M., Dixon, N.E. and van Oijen, A.M. (2020). A Primase-Induced Conformational Switch Controls the Stability of the Bacterial Replisome. *Molecular Cell*, [online] 79(1), pp.140-154.e7. doi:https://doi.org/10.1016/j.molcel.2020.04.037.

Nudler, E. (2012). RNA Polymerase Backtracking in Gene Regulation and Genome Instability. *Cell*, 149(7), pp.1438–1445. doi:https://doi.org/10.1016/j.cell.2012.06.003.

O'Donnell, M., Langston, L. and Stillman, B. (2013). Principles and Concepts of DNA Replication in Bacteria, Archaea, and Eukarya. *Cold Spring Harbor Perspectives in Biology*, [online] 5(7), pp.a010108–a010108. doi:https://doi.org/10.1101/cshperspect.a010108.

Ozawa, K., Horan, N.P., Robinson, A., Yagi, H., Hill, F., Slobodan Jergic, Xu, Z.-Q., Loscha, K.V., Li, N., Moeava Tehei, Oakley, A.J., Otting, G., Huber, T. and Dixon, N.E. (2013). Proofreading exonuclease on a tether: the complex between the E. coli DNA polymerase III subunits α, ε, θ and β reveals a highly flexible arrangement of the proofreading domain. *Nucleic Acids Research*, 41(10), pp.5354–5367. doi:https://doi.org/10.1093/nar/gkt162.

Payne, I., I.C. van Knippenberg, Bell, H., Filipe, S.R., Sherratt, D.J. and McGlynn, P. (2006). Replication fork blockage by transcription factor-DNA complexes in Escherichia coli. *Nucleic Acids Research*, 34(18), pp.5194–5202. doi:https://doi.org/10.1093/nar/gkl682.

Perederina, A., Svetlov, V., Vassylyeva, M.N., Tahirov, T.H., Yokoyama, S., Artsimovitch, I. and Vassylyev, D.G. (2004). Regulation through the Secondary Channel—Structural Framework for ppGpp-DksA Synergism during Transcription. *Cell*, 118(3), pp.297–309. doi:https://doi.org/10.1016/j.cell.2004.06.030.

Plank, M., Wadhams, G.H. and Leake, M.C. (2009). Millisecond timescale slimfield imaging and automated quantification of single fluorescent protein molecules for use in probing complex biological processes. *Integrative Biology*, 1(10), p.602. doi:https://doi.org/10.1039/b907837a.

Po Jui Chen, McMullin, A.B., Visser, B.J., Mei, Q., Rosenberg, S.M. and Bates, D. (2023). *Interdependent progression of bidirectional sister replisomes in E. coli*. [online] eLife. Available at: https://elifesciences.org/articles/82241 [Accessed 15 Sep. 2024].

Pomerantz, R.T. and O'Donnell, M. (2008). The replisome uses mRNA as a primer after colliding with RNA polymerase. *Nature*, 456(7223), pp.762–766. doi:https://doi.org/10.1038/nature07527.

Prescott, D.M. and Kuempel, P.L. (1972). Bidirectional Replication of the Chromosome in *Escherichia coli*. *PNAS*, [online] 69(10), pp.2842–2845. doi:https://doi.org/10.1073/pnas.69.10.2842.

Reyes-Lamothe, R., Possoz, C., Danilova, O. and Sherratt, D.J. (2008). Independent Positioning and Action of Escherichia coli Replisomes in Live Cells. *Cell*, 133(1), pp.90–102. doi:https://doi.org/10.1016/j.cell.2008.01.044.

Reyes-Lamothe, R., Sherratt, D.J. and Leake, M.C. (2010). Stoichiometry and Architecture of Active DNA Replication Machinery in Escherichia coli. *Science*, 328(5977), pp.498–501. doi:https://doi.org/10.1126/science.1185757.

Robinson, A., J. Causer, R. and E. Dixon, N. (2012). Architecture and Conservation of the Bacterial DNA Replication Machinery, an Underexploited Drug Target. *Current Drug Targets*, 13(3), pp.352–372. doi:https://doi.org/10.2174/138945012799424598.

Rutkauskas, D., Zhan, H., Matthews, K.S., Pavone, F.S. and Vanzi, F. (2009). Tetramer opening in LacI-mediated DNA looping. *Proceedings of the National Academy of Sciences*, [online] 106(39), pp.16627–16632. doi:https://doi.org/10.1073/pnas.0904617106.

Sandler, S.J., Leroux, M., Windgassen, T.A. and Keck, J.L. (2021). *Escherichia coli* K-12 has two distinguishable PriA-PriB replication restart pathways. *Molecular Microbiology*, 116(4), pp.1140–1150. doi:https://doi.org/10.1111/mmi.14802.

Sandler, S.J., Marians, K.J., Zavitz, K.H., Coutu, J., Parent, M.A. and Clark, A.J. (1999). dnaC mutations suppress defects in DNA replication- and recombination-associated functions in

priB and priC double mutants in Escherichia coli K-12. *Molecular Microbiology*, 34(1), pp.91–101. doi:https://doi.org/10.1046/j.1365-2958.1999.01576.x.

Sankar, T.S., Wastuwidyaningtyas, B.D., Dong, Y., Lewis, S.A. and Wang, J.D. (2016). The nature of mutations induced by replication–transcription collisions. *Nature*, 535(7610), pp.178–181. doi:https://doi.org/10.1038/nature18316.

Santos, J.A. and Lamers, M.H. (2020). Novel Antibiotics Targeting Bacterial Replicative DNA Polymerases. *Antibiotics*, 9(11), p.776. doi:https://doi.org/10.3390/antibiotics9110776.

Shaner, N.C., Campbell, R.E., Steinbach, P.A., Giepmans, B.N.G., Palmer, A.E. and Tsien, R.Y. (2004). Improved monomeric red, orange and yellow fluorescent proteins derived from Discosoma sp. red fluorescent protein. Nature Biotechnology, 22(12), pp.1567–1572. doi:https://doi.org/10.1038/nbt1037.

Spinks, R.R., Spenkelink, L.M., Stratmann, S.A., Xu, Z.-Q., Stamford, N., Brown, S.E., Dixon, N.E., Jergic, S. and van Oijen, A.M. (2021). DnaB helicase dynamics in bacterial DNA replication resolved by single-molecule studies. *Nucleic Acids Research*, [online] 49(12), pp.6804–6816. doi:https://doi.org/10.1093/nar/gkab493.

Srivatsan, A., Tehranchi, A., MacAlpine, D.M. and Wang, J.D. (2010). Co-Orientation of Replication and Transcription Preserves Genome Integrity. *PLoS Genetics*, 6(1), p.e1000810. doi:https://doi.org/10.1371/journal.pgen.1000810.

Szymanski, M.R., Jezewska, M.J. and Bujalowski, W. (2013). The*Escherichia coli*Primosomal DnaT Protein Exists in Solution as a Monomer–Trimer Equilibrium System. *Biochemistry*, 52(11), pp.1845–1857. doi:https://doi.org/10.1021/bi301568w.

Taft-Benz, S.A. and Schaaper, R.M. (2004). The Subunit of Escherichia coli DNA Polymerase III: a Role in Stabilizing the Proofreading Subunit. *Journal of Bacteriology*, 186(9), pp.2774–2780. doi:https://doi.org/10.1128/jb.186.9.2774-2780.2004.

Tehranchi, A.K., Blankschien, M.D., Zhang, Y., Halliday, J.A., Srivatsan, A., Peng, J., Herman, C. and Wang, J.D. (2010). The Transcription Factor DksA Prevents Conflicts between DNA

Replication and Transcription Machinery. *Cell*, 141(4), pp.595–605. doi:https://doi.org/10.1016/j.cell.2010.03.036.

Wechsler, J.A. (1975). Genetic and phenotypic characterization of dnaC mutations. *Journal of Bacteriology*, 121(2), pp.594–599. doi:https://doi.org/10.1128/jb.121.2.594-599.1975.

Wolak, C., Jiang, H., Soubry, N., Sandler, S.J., Reyes-Lamothe, R. and Keck, J.L. (2020). Interaction with single-stranded DNA-binding protein localizes ribonuclease HI to DNA replication forks and facilitates R-loop removal. *Molecular Microbiology*, 114(3), pp.495–509. doi:https://doi.org/10.1111/mmi.14529.

Wollman , A., Syeda, A.H., Howard, J., Payne-Dwyer, A., Leech, A., Dominika Warecka, Guy, C., McGlynn, P., Hawkins, M. and Leake, M.C. (2021). Tetrameric UvrD helicase is located at the*E. coli replisome* due to frequent replication blocks. *bioRxiv (Cold Spring Harbor Laboratory)*. doi:https://doi.org/10.1101/2021.02.22.432310.